ESC-TR-92-203

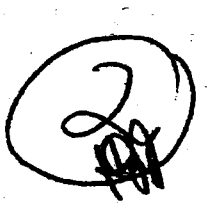

Technical Report
977

Experimental Evaluation of an Adaptive Focusing Algorithm for a Microwave Planar Phased-Array Hyperthermia System at UCSF

A.J. Fenn
C.J. Diederich
P.R. Stauffer

17 May 1993

Lincoln Laboratory
MASSACHUSETTS INSTITUTE OF TECHNOLOGY
LEXINGTON, MASSACHUSETTS

Prepared for the Department of the Air Force under Contract F19628-90-C-0002.

DISCLAIMER NOTICE

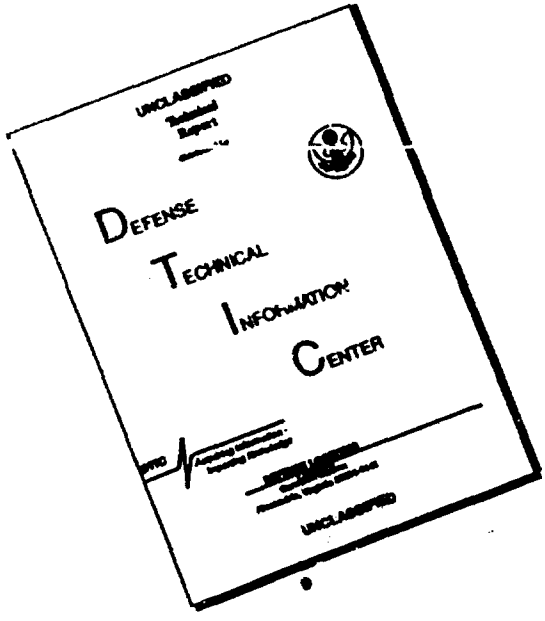

THIS DOCUMENT IS BEST QUALITY AVAILABLE. THE COPY FURNISHED TO DTIC CONTAINED A SIGNIFICANT NUMBER OF PAGES WHICH DO NOT REPRODUCE LEGIBLY.

MASSACHUSETTS INSTITUTE OF TECHNOLOGY
LINCOLN LABORATORY

EXPERIMENTAL EVALUATION OF AN ADAPTIVE FOCUSING ALGORITHM FOR A MICROWAVE PLANAR PHASED-ARRAY HYPERTHERMIA SYSTEM AT UCSF

A.J. FENN
Group 63

C.J. DIEDERICH
P.R. STAUFFER
University of California at San Francisco

TECHNICAL REPORT 977

17 MAY 1993

LEXINGTON **MASSACHUSETTS**

ABSTRACT

An adaptive focusing microwave planar phased-array hyperthermia system for improved heating of superficial tumors is experimentally investigated. A commercial microwave hyperthermia planar phased-array antenna system at the University of California at San Francisco (UCSF) Radiation Oncology Department has been modified to implement a gradient-search adaptive focusing algorithm. Adaptive focusing measurements in a muscle-equivalent liquid phantom with a 915-MHz microwave planar phased-array hyperthermia system comprising 16 independent amplitude/phase-controlled waveguide antenna elements (Microtherm-1000, Labthermics Technologies, Inc., Champaign, IL) are reported. An electric-(E-)field feedback probe detector, fabricated at UCSF, measured the E-field generated by the hyperthermia phased array. A method of steepest-ascent gradient-search feedback algorithm, implemented in software, controls the hyperthermia array phase shifters and focuses the transmitted radiation beam. In 10 to 15 iterations, the measured phantom data indicate rapid convergence of the adaptive focusing algorithm and significant increase of the focal region field strength due to the adaptive focusing. Two-dimensional E-field radiation pattern measurements were collected by scanning the E-field dipole probe antenna inside the muscle-equivalent liquid phantom. The measured, adaptively phase-focused radiation pattern data indicate a maximum useful heating depth of about 3 cm in a muscle-equivalent sugar/saline phantom having dielectric losses of 3 dB/cm.

ACKNOWLEDGMENTS

Technical discussions with Dr. Everette C. Burdette are appreciated.

TABLE OF CONTENTS

Abstract	iii
Acknowledgments	v
List of Illustrations	ix
1. INTRODUCTION	1
2. THEORY	7
2.1 Adaptive Focusing/Nulling Hyperthermia System Concept	7
2.2 Adaptive Transmit-Array Formulation	7
2.3 System Considerations	15
3. MATERIALS AND METHODS	17
4. MEASURED RESULTS	21
4.1 Review of Earlier Investigations at UCSF	21
4.2 New Measurements at UCSF	25
5. CONCLUSION	33
APPENDIX A - Measured E-Field Probe Raw Data	35
REFERENCES	37

LIST OF ILLUSTRATIONS

Figure No.		Page
1	The 915-MHz microwave planar phased-array hyperthermia system used in experiments at the UCSF Hyperthermia Laboratory.	3
2	The 915-MHz microwave planar phased-array applicator used in the Labthermics Microtherm-1000 system.	4
3	Adaptive focusing/nulling hyperthermia system concept.	8
4	Scatter diagram in rectangular coordinates for the amplitude and phase of the transmit weights in a hyperthermia phased-array antenna.	10
5	Figure of merit with transmit-weight dithering for optimum search directions.	14
6	Gradient-search algorithm block diagram for adaptive focusing hyperthermia system.	16
7	The 915-MHz microwave planar phased-array applicator used in the Labthermics Microtherm-1000 system.	18
8	UCSF/MIT adaptive hyperthermia experiments equipment.	19
9	Amplifier circuit for E-field probe.	19
10	Dipole probe, probe (x, y, z) positioner system, and the muscle-equivalent phantom tank.	20
11	Measured E-field radiation pattern for Microtherm-1000 planar phased array focused in different media.	22
12	UCSF experimental test set-up for in vivo measurements of pig thigh.	23
13	Measured E-field radiation pattern for Microtherm-1000 planar phased array illuminating muscle-equivalent liquid phantom.	24
14	Comparison of measured SAR and temperature distributions for Microtherm-1000 system focused at 2.5 cm in pig thigh.	26
15	Comparison of measured two-dimensional radiation patterns of the Microtherm-1000 with focal depth of 8 cm in deionized water phantom.	27
16	Measured two-dimensional radiation pattern of the Microtherm-1000 using MIT Lincoln Laboratory adaptive focusing algorithm with 4-cm focal depth in muscle-equivalent liquid phantom (uniform illumination).	28

LIST OF ILLUSTRATIONS
(Continued)

Figure No.		Page
17	Measured two-dimensional radiation pattern of the Microtherm-1000 using MIT Lincoln Laboratory adaptive focusing algorithm with 4-cm focal depth in muscle-equivalent liquid phantom (adjusted uniform illumination).	29
18	Measured two-dimensional radiation pattern of the Microtherm-1000 using MIT Lincoln Laboratory adaptive focusing algorithm with 4-cm focal depth in muscle-equivalent liquid phantom (inverse taper illumination).	30
19	Measured E-field focused at $z = 4$ cm as a function of adaptive phase focusing gradient-search iteration number for a muscle-equivalent liquid phantom.	31

1. INTRODUCTION

Adaptive array antennas are well known for their ability to improve, in real time, the performance of communications and radar systems [1–4]. Recently, adaptive array techniques have been applied to the medical use of radio frequency (RF) hyperthermia for deep-seated tumor therapy [5–12]. With an adaptive RF or microwave hyperthermia array, it is possible to automatically control the electric- (E-)field at multiple positions within the target body [5–12]. The E-field radiated by a hyperthermia phased array can be minimized (nulled) and maximized (focused) at desired target positions by adaptively adjusting the transmit amplifiers and phase shifters of the hyperthermia apparatus. Multiple adaptive E-field nulls and adaptive focusing were experimentally demonstrated at the State University of New York (SUNY) Health Science Center with a modified commercial RF hyperthermia phased-array system and phantom target measurements [9–12]. An annular phased-array antenna (BSD-Medical Corp., Sigma-60 [13–14]), operating at $\approx$ 100 MHz, was used [9–12]. This report investigates a 915-MHz, planar phased-array antenna hyperthermia applicator via adaptive focusing experiments at the University of California at San Francisco (UCSF).

Treating a patient's malignant tumors is often a difficult task. The objective of the treatment is to reduce or completely remove the tumor mass by one or more modalities available at the treatment facility, commonly surgery, chemo-, and x-ray therapy [15]. One particular method used by itself or in conjunction with another is "tissue heating" or hyperthermia [15–19], a form of high fever. A controlled thermal dose distribution is required for hyperthermia to be a valuable therapy. Typical localized hyperthermia temperatures required for therapeutic treatment of cancer are in the 42.5° to 45°C range. Normal tissue should be kept at temperatures below 42.5°C during treatment. The most difficult aspect of implementing hyperthermia with either RF or acoustic (ultrasound) waves is producing sufficient heating at depth. Multiple-applicator RF hyperthermia arrays are commonly used to provide a focused main beam at the tumor position. A focal region should be concentrated at the tumor with minimal energy delivered to surrounding normal tissue. As the hyperthermia antenna beamwidth is proportional to the wavelength, a small focal region suggests that the RF wavelength be as small as possible. Due to propagation losses in tissue, however, RF penetration depth decreases with increasing transmit frequency. Typically, noninvasive phased arrays operating close to 100 MHz are suggested for deep-seated and 915-MHz arrays for shallow tumor heating. One of the major problems in heating a tumor with a hyperthermia antenna is the formation of undesired hot spots in surrounding tissue, which often produces pain, burns, and blistering in the patient, requiring terminating the treatment. Thus techniques for reducing hot spots are necessary.

A typical clinical RF or microwave hyperthermia treatment consists of several two-hour sessions spread over a period of weeks. The patient is prepared during the first hour of the session—temperature and vital signs monitoring instrumentation are interfaced with the patient, the hyperthermia antenna microwave signal generator is turned on, and the tumor is heated by radiated electromagnetic energy. The tumor should be heated for $\approx$ 45 min at a temperature of 42.5° to 45°C. Prior to the actual delivery of microwave energy to the tumor, $\approx$ 15 min (maximum) is

available to manually or adaptively shape the microwave E-field distribution within patient target tissue. Current clinical operation of commercial hyperthermia phased arrays allows limited manual control of the array transmit element amplitude and phase. Some improvement in the E-field distribution can be achieved by this manual trial-and-error method, but automatic adjustment techniques, offered by adaptive arrays, are desirable and possibly offer better E-field distributions.

Several journals have published special issues on acoustic and electromagnetic hyperthermia treatment of cancer [20–22]. Studies have been conducted to produce improved therapeutic field distributions with hyperthermia phased arrays [23–42]. Phase control can synthesize improved RF radiation patterns without adaptive control of the transmit-array weights [23–28]. Array transmit weights (defined here as amplitude and phase states associated with a transmit channel) can be adaptively controlled to maximize tumor temperature (or microwave power delivered to the tumor), while minimizing the surrounding tissue temperature (or RF power delivered to the surrounding tissue) [29–42]. Ultrasound receive feedback sensors [41,42] and a pseudoinverse pattern synthesis method [43] generate multiple focal points for a phased-array hyperthermia applicator. Previous reports [5,9] and several conference articles [6–8] investigate the theoretical benefit of using adaptive nulling with noninvasive auxiliary dipole sensors to reduce the E-field intensity at selected positions in the target body while maintaining a desired focus at a tumor. Multiple adaptive E-field nulls were used to show a theoretical reduction in hot spots for a homogeneous elliptical phantom target surrounded by a water bolus and hyperthermia ring array [6–8].

Microwave antenna applicators are often considered for inducing localized hyperthermia to superficial tumors located on the chest wall and head and neck regions. The power deposition patterns (also referred to as the specific absorption rate or SAR)[1] of single aperture applicators are often limited to effective heating well within the aperture boundaries [44–47]. With 915-MHz microwave radiation, waveguide applicators have a limited heating depth to less than 3 cm and lateral heating dimensions of 3 to 5 cm, which is smaller than needed to cover many tumors [48]. Heating depth is limited to only about 3 cm because at 915 MHz the dielectric loss in tissue is typically 3 dB/cm. A predictor of good local heating control is to use the 50% iso-SAR coverage (laterally and with depth) of the tumor [49]. Several methods for improving the SAR heating patterns of single-aperture hyperthermia devices are under investigation. For example, microwave absorbing saline-filled boluses can shape the heating pattern of a waveguide applicator as demonstrated in Sherar et al. [50]. Mechanically scanned microwave applicators have been used to shape the power deposition pattern [48,51,52]. Phased-array applicators can shape the power deposition pattern produced by planar [48,51,53,54] and conformal arrays [55,56]. Studies to improve penetration depth with phased arrays by controlling the phase and amplitude of each array element have been conducted [53,54,57].

---

[1] SAR $= \frac{1}{2}\sigma|E|^2/\rho$, where E is the E-field, σ is the electric conductivity of the tissue, and ρ is its density.

The Microtherm-1000 (Labthermics Technologies, Inc., Champaign, IL) hyperthermia microwave planar phased-array antenna system used in these experiments is shown in Figure 1. By

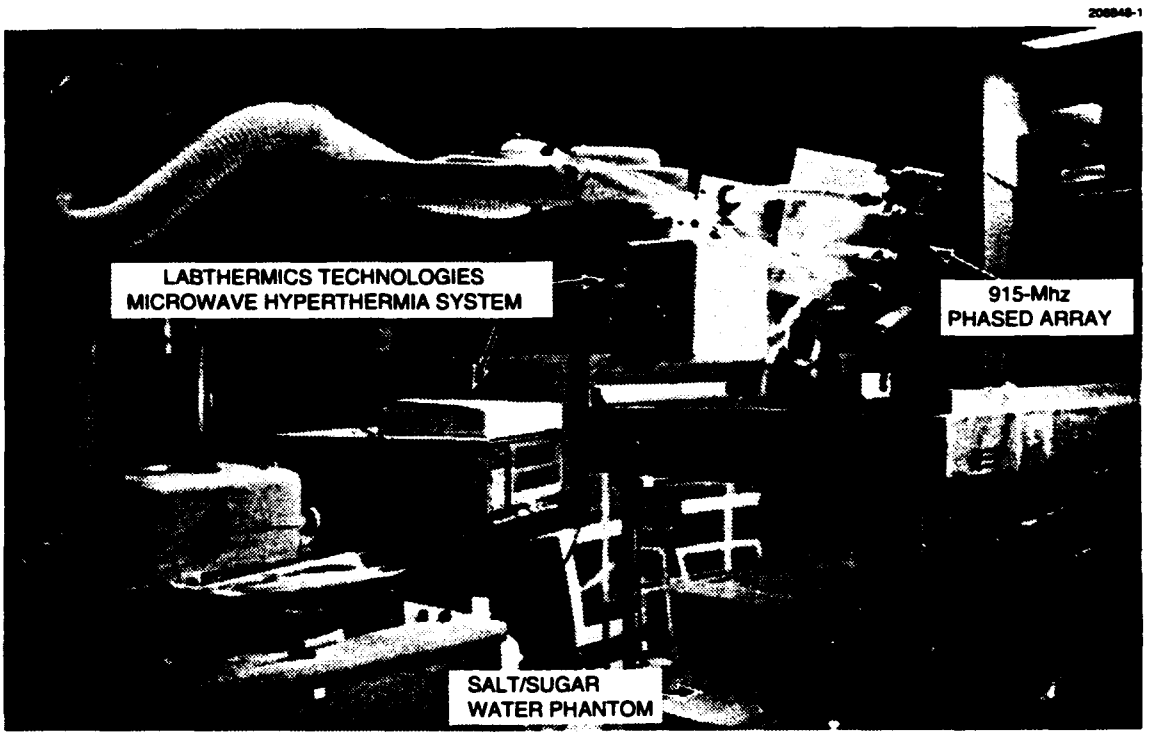

Figure 1. The 915-MHz microwave planar phased-array hyperthermia system used in experiments at the UCSF Hyperthermia Laboratory.

transmitting close to the patient with a planar phased array, it is possible to obtain superficial heating over large ($\approx$ 15 x 15 cm) as well as small ($\approx$ 3.5 x 3.5 cm) areas, depending on the array amplitude illumination function. In Figure 2, the Microtherm-1000 uses a 15- x 15-cm planar array with 16 square waveguide elements operating at 915 MHz. The 16 independent variable power amplifiers drive the waveguides, and each of the 16 active channels has an electronically controlled variable-phase shifter to focus the array. A cool-water bolus between the patient and the phased array prevents excess heating of the skin surface. The bolus is filled with circulating deionized water, which has a very low microwave propagation loss of about 0.3 dB/cm.

A candidate adaptive focusing algorithm proposed by MIT Lincoln Laboratory for use in hyperthermia is a gradient search based on maximizing the signal received by an E-field sensor

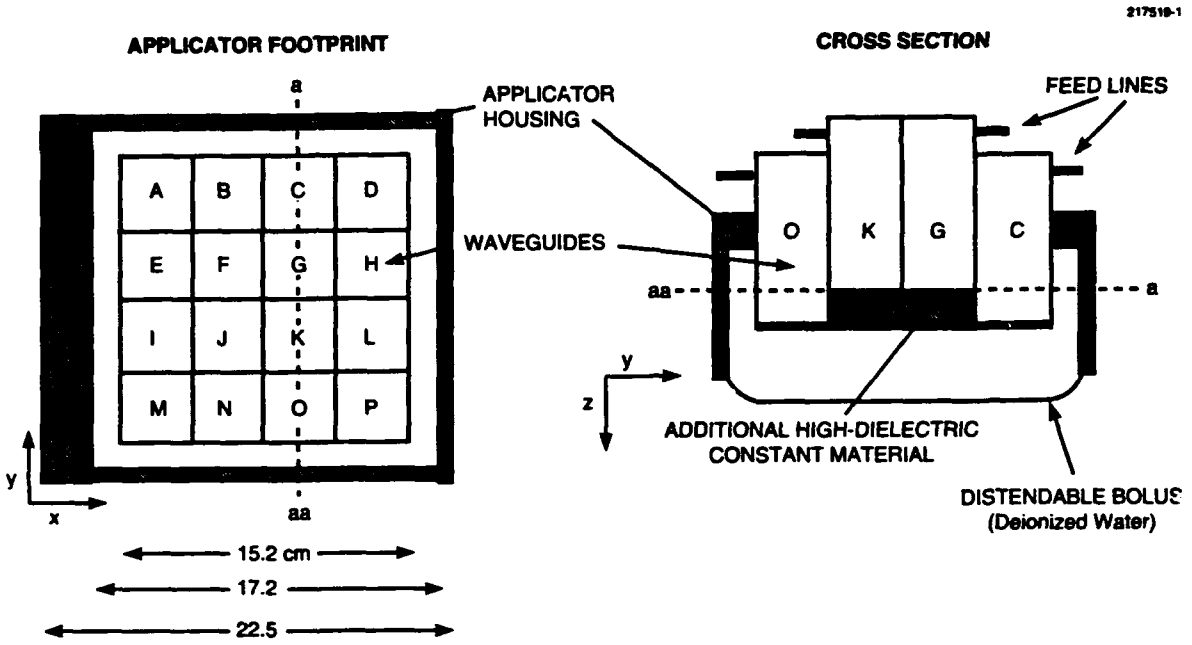

Figure 2. The 915-MHz microwave planar phased-array applicator used in the Labthermics Microtherm-1000 system.

positioned within a tumor. UCSF has recently evaluated (with experiments in phantoms and animals) a systematic search, iterative focusing algorithm for phased-array hyperthermia [58]. Note that the E-field probe used in the UCSF measurements is a short dipole with a semiconductor diode detector [59–62]. A particular concept of adaptive focusing as it applies to hyperthermia follows.

Recently, a technique called focused near-field adaptive nulling [63–70] was investigated to test the performance of radar and communications systems. A calibration probe antenna focuses the main beam at approximately one diameter D of the phased array. Additional (auxiliary) probe antennas are located in the sidelobe region of the phased-array quiescent radiation pattern. Adaptive nulls are formed in the direction of these auxiliary probes. Computer simulations show that a radar system can be tested by using the focused near-field nulling technique [68,70]; experimental measurements of focused near-field adaptive nulling have been performed [69]. For the radar system, interference signals entering through uncontrolled sidelobes can reduce the signal-to-noise ratio (SNR); adaptive nulling [1–4] counteracts this possible degradation. In the hyperthermia system, high-transmit antenna E-field strengths can create hot spots in the target tissue. These high-temperature regions can possibly be alleviated with adaptive nulling of the E-field at specified positions on the surface of or inside the target.

Consider a potential clinical application of the proposed adaptive hyperthermia system. The Microtherm-1000 currently does not supply E-field probes to monitor clinical hyperthermia treatments; however, as current measurements indicate, an E-field probe could be added to this system to provide feedback signals to the adaptive algorithm. In theory, with 16 independent transmit channels, the E-field radiation pattern can be controlled at up to 16 points (in the radiation field), using a feedback signal measured at each point.

The remainder of this report is organized as follows. Section 2 discusses the concept for an adaptive focusing hyperthermia system and describes in detail the gradient-search feedback algorithm implementing the adaptive array. Section 3 describes the materials and methods used to obtain the measured adaptive focusing results in a phantom target. Section 4 gives measured results for an adaptive focusing, hyperthermia planar phased array operating at a CW frequency of 915 MHz. The measured received microwave power distributions at the intended focus, before and after adaptive focusing with a short-dipole field probe, are presented. Limited two-dimensional E-field radiation patterns are also shown. Section 5 presents conclusions.

2. THEORY

2.1 Adaptive Focusing/Nulling Hyperthermia System Concept

The concept of an adaptive focusing/nulling hyperthermia system is shown in Figure 3. Theoretically, to generate the desired field distribution in a clinical adaptive hyperthermia system, receiving sensors are positioned as closely as possible to the focus (tumor site) and where high temperatures are to be avoided (such as near vital organs and scar tissue). A noninvasive adaptive nulling system is achieved by placing auxiliary sensors $1, 2, \cdots, N_{aux}$ on the target skin as shown. (With 915-MHz microwave radiation as considered in this report, hot spots, if present, are expected to occur near the target surface.) The null zones centered at each auxiliary probe naturally extend into the target region to eliminate undesired hot spots. The width of each null zone is directly related to the strength of each null (sometimes referred to as the "amount of cancellation"), which is directly related to the SNR at the sensor position. A low SNR produces a small amount of nulling, a high SNR produces a large amount. Resolution (minimum spacing between the focus and null positions) is normally equal to the half-power beamwidth of the antenna and is enhanced somewhat by using weak nulls whenever the separation between the null and focus is closer than the half-power beamwidth.

Initially, the hyperthermia array is focused to produce the required field intensity at the tumor. An invasive probe is required to achieve the optimum focus at depth. To avoid hot spots, it is necessary to minimize the power received at the desired null positions and to constrain the array weights to deliver a required amount of transmitted or focal region power. The adaptive-array weights (with amplitude A and phase Φ) are controlled by the gradient-search algorithm to rapidly form the focused beam before a significant amount of target heating takes place. With this adaptive technique, it should be possible to avoid hot spots and maintain a therapeutic thermal dose at the tumor.

2.2 Adaptive Transmit-Array Formulation

Consider a hyperthermia array with N antenna elements, where $N = 16$ for the Microtherm-1000 system. The input signal to each of the N array elements is obtained from the amplitude and phase-adjusted signal distributed by a power divider network. The number of adaptive channels is assumed to be equal to the number of transmit antennas N. Let $\boldsymbol{w} = (w_1, w_2, \cdots, w_N)^T$ (superscript T = transpose) denote the adaptive channel weight vector as shown in Figure 3.

Commonly, the weight vector is constrained to deliver a required amount of power to the hyperthermia array or the tumor. For simplicity in the experimental adaptive hyperthermia array control software, the weights are constrained such that

$$\sum_{n=1}^{N} |w_n|^2 = K \quad , \tag{1}$$

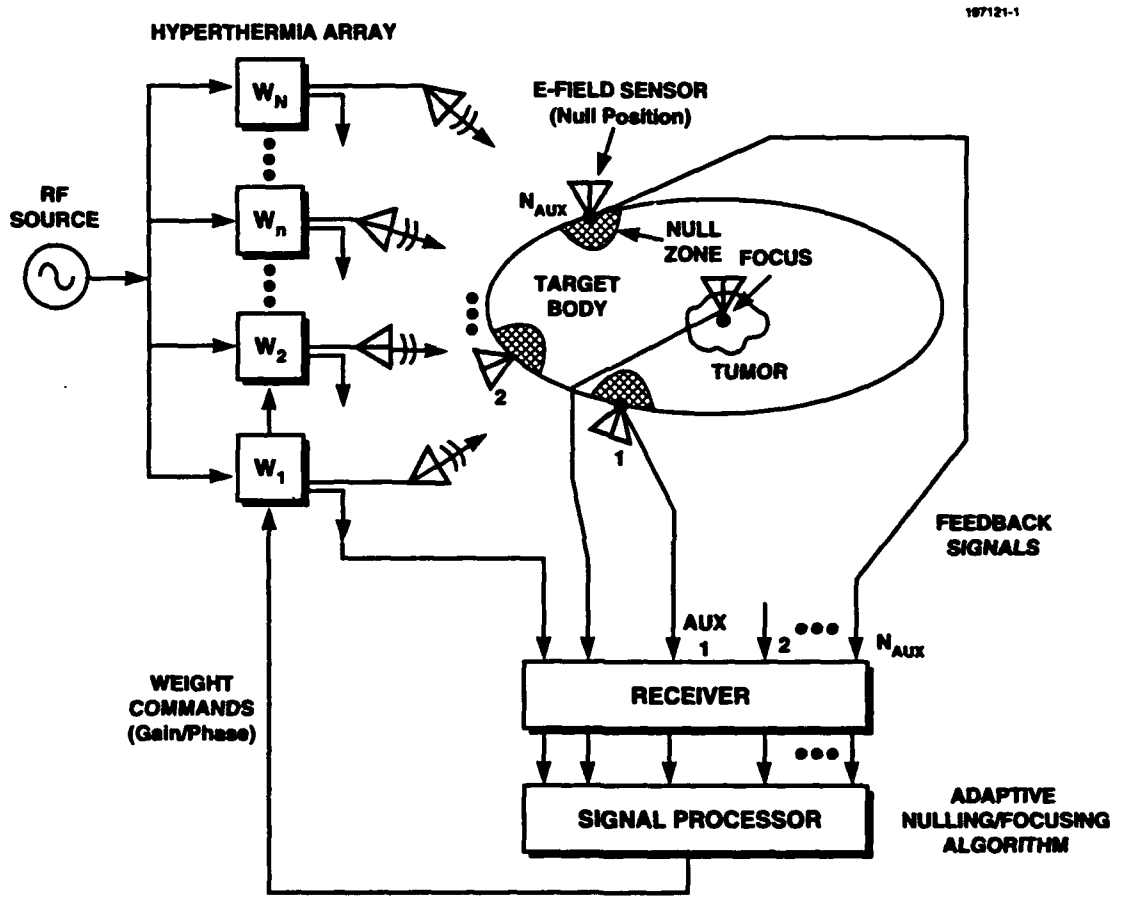

Figure 3. Adaptive focusing/nulling hyperthermia system concept.

where $|w_n|$ is the transmit-weight amplitude for the nth adaptive channel and K is a constant. To generate an adaptive phase focus, a gradient-search algorithm controls the transmit weights (phase shifters).

2.2.1 Gradient-Search Algorithm

Gradient-search algorithms are commonly used in adaptive-array applications, particularly where the channel-to-channel correlation cannot be calculated or measured. With a gradient search, only the output power of the receiver channels is measured and used as a feedback signal to the algorithm. A wide variety of gradient searches exists [71–76]; this report uses a standard method of steepest descent [71,77].

In the Microtherm-1000 system at UCSF, only the received E-field power is measured, hence it is appropriate to consider a gradient-search algorithm to control the E-field power at selected positions. Gradient search controls the transmit weights iteratively so that the microwave signal received by the probe-array is maximized (focused). Transmit-array phase shifters are adaptively changed in small increments and probe-array output power is monitored to determine phase settings that increase the output power most rapidly to a maximum. The mathematical formulation for the gradient search is straightforward [71,77] and is next described in the context of hyperthermia [9]. Although the formulation is given as a maximization problem, the equations are readily converted to the minimization problem. Considered here is the general mathematical formulation of amplitude and phase dithering; however, only the phase-dithering approach is applied in the adaptive focusing experiments.

The summation of power received at the E-field probe(s) is denoted p^{rec}. The adaptive-array signal enhancement ratio C is defined here as the ratio of the summation of probe-received power after adaption p_a to the summation of probe-received power before adaption p_b; that is,

$$C = \frac{p_a}{p_b} \quad . \tag{2}$$

Consider now J sets (or iterations) of N transmit weights that are applied to an adaptive hyperthermia phased-array antenna. In terms of adaptive focusing, the optimum transmit-weight settings (from the collection of J sets of N transmit weights) occur when the total power received by the auxiliary probe array, denoted p^{rec}, is maximized. For notational convenience let a figure of merit F denote p^{rec} and employ a method of steepest-ascent gradient search to find the optimum transmit weights to maximize F; that is,

$$F_{opt} = max(F_j) \;\; j = 1,2,\cdots,J \quad . \tag{3}$$

Ideally, in the adaptive focusing gradient search, power should increase after each iteration, that is, $F_2 > F_1$, $F_3 > F_2$, $F_4 > F_3$, $\cdots$, $F_J > F_{J-1}$. Due to system noise, however, this ideal

behavior may not always be achieved. Assume that there are N complex transmit weights in the hyperthermia phased array as suggested by the amplitude and phase scatter diagram depicted in Figure 4. The nth transmit weight in the jth configuration (or iteration) of transmit weights is denoted

$$w_{nj} = A_{nj}e^{j\Phi_{nj}} \quad , \tag{4}$$

where A_{nj} is the transmit-weight amplitude distributed over the range A_{min} to A_{max} and Φ_{nj} is the transmit-weight phase distributed over the range Φ_{min} to Φ_{max}. The goal is to find the values of amplitude and phase for each of the N transmit weights such that F is maximized, and an adaptive radiation pattern peak(s) is formed at the auxiliary sensor position(s).

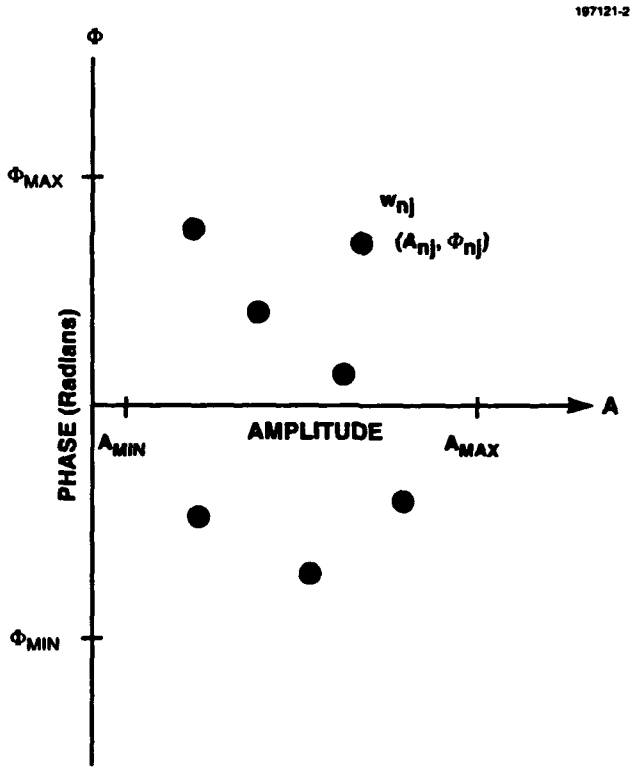

Figure 4. Scatter diagram in rectangular coordinates for the amplitude and phase of the transmit weights in a hyperthermia phased-array antenna. The nth transmit weight in the jth configuration of transmit weights is denoted w_{nj}.

Assuming an initial setting of the N transmit weights, the weights are adjusted by dithering them until the optimum F is achieved. The goal is to find the collective search directions for the N transmit weights such that F increases most rapidly; that is, transmit weights are selected so that the directional derivative is maximized at $(\mathbf{A}_j, \Phi_j)$, where $\mathbf{A}_j$ and Φ_j are the amplitude and phase column vectors, respectively.

The directional derivative of F_j is expressed in terms of the amplitude and phase changes of the transmit weights as

$$D(F_j) = \sum_{n=1}^{N} \left(\frac{\partial F_j}{\partial A_{nj}} r_{Anj} + \frac{\partial F_j}{\partial \Phi_{nj}} r_{\Phi nj}\right) \quad , \tag{5}$$

where ∂ means partial derivative and $r_{Anj}, r_{\Phi nj}$ are the (A, Φ) directions for which F_j is increasing most rapidly. The directions $r_{Anj}, r_{\Phi nj}$ are constrained by

$$\sum_{n=1}^{N} (r_{Anj}^2 + r_{\Phi nj}^2) = 1 \quad . \tag{6}$$

The goal is to maximize $D(F_j)$ subject to Equation (6). Using Lagrange multipliers, construct the Lagrangian function

$$L_j = \sum_{n=1}^{N} \left(\frac{\partial F_j}{\partial A_{nj}} r_{Anj} + \frac{\partial F_j}{\partial \Phi_{nj}} r_{\Phi nj}\right) + G[1 - \sum_{n=1}^{N} (r_{Anj}^2 + r_{\Phi nj}^2)] \quad , \tag{7}$$

where G is a constant to be determined. The requirement that L_j be an extremum implies

$$\frac{\partial L_j}{\partial r_{Anj}} = \frac{\partial F_j}{\partial A_{nj}} - 2G r_{Anj} = 0 \quad , n = 1, 2, \cdots, N \tag{8}$$

$$\frac{\partial L_j}{\partial r_{\Phi nj}} = \frac{\partial F_j}{\partial \Phi_{nj}} - 2G r_{\Phi nj} = 0 \quad , n = 1, 2, \cdots, N \quad , \tag{9}$$

or

$$r_{Anj} = \frac{1}{2G} \frac{\partial F_j}{\partial A_{nj}} \tag{10}$$

$$r_{\Phi nj} = \frac{1}{2G} \frac{\partial F_j}{\partial \Phi_{nj}} \quad . \tag{11}$$

Squaring Equations (10) and (11) and invoking Equation (6) yields

$$\sum_{n=1}^{N}(\tau_{Anj}^2+\tau_{\Phi nj}^2)=1=\frac{1}{4G^2}\sum_{n=1}^{N}[(\frac{\partial F_j}{\partial A_{nj}})^2+(\frac{\partial F_j}{\partial \Phi_{nj}})^2] \quad ; \tag{12}$$

thus,

$$G=\pm\frac{1}{2}\sqrt{\sum_{n=1}^{N}[(\frac{\partial F_j}{\partial A_{nj}})^2+(\frac{\partial F_j}{\partial \Phi_{nj}})^2]} \quad . \tag{13}$$

Substituting Equation (13) into Equations (10) and (11) gives

$$\tau_{Anj}=+\frac{\frac{\partial F_j}{\partial A_{nj}}}{\sqrt{\sum_{n=1}^{N}[(\frac{\partial F_j}{\partial A_{nj}})^2+(\frac{\partial F_j}{\partial \Phi_{nj}})^2]}} \tag{14}$$

$$\tau_{\Phi nj}=+\frac{\frac{\partial F_j}{\partial \Phi_{nj}}}{\sqrt{\sum_{n=1}^{N}[(\frac{\partial F_j}{\partial A_{nj}})^2+(\frac{\partial F_j}{\partial \Phi_{nj}})^2]}} \quad . \tag{15}$$

In Equations (14) and (15) the plus sign was chosen corresponding to the direction of maximum function increase. By changing the plus to a minus in Equations (14) and (15), the search directions then correspond to the direction of maximum function decrease, i.e., the minus sign minimizes the power delivered away from the focus or tumor site. Partial derivatives

$$\frac{\partial F_j}{\partial A_{nj}},\frac{\partial F_j}{\partial \Phi_{nj}} \quad ;n=1,2,\cdots,N \tag{16}$$

represent the gradient directions for maximum function increase.

Because F is measured and cannot be expressed in analytical form, the partial derivatives are numerically evaluated using finite differences. Thus

$$\frac{\partial F_j}{\partial A_{nj}}=\frac{\Delta F_{Anj}}{2\Delta A_{nj}} \tag{17}$$

$$\frac{\partial F_j}{\partial \Phi_{nj}}=\frac{\Delta F_{\Phi nj}}{2\Delta \Phi_{nj}} \quad , \tag{18}$$

where, as shown in Figure 5,

$$\Delta F_{Anj} = F_j(A_{nj} + \Delta A_{nj}; \Phi_{nj}) - F_j(A_{nj} - \Delta A_{nj}; \Phi_{nj}) \quad , \tag{19}$$

$$\Delta F_{\Phi nj} = F_j(A_{nj}; \Phi_{nj} + \Delta \Phi_{nj}) - F_j(A_{nj}; \Phi_{nj} - \Delta \Phi_{nj}) \tag{20}$$

and ΔA_{nj} and $\Delta \Phi_{nj}$ are the maximum step sizes. Assume for now that the increments ΔA_{nj} and $\Delta \Phi_{nj}$ depend on the iteration number j and transmit element index n. Substituting Equations (19) and (20) into (17) and (18) and then substituting the result into (14) and (15) gives the desired result for the search directions

$$r_{Anj} = \frac{\frac{\Delta F_{Anj}}{\Delta A_{nj}}}{\sqrt{\sum_{n=1}^{N}[(\frac{\Delta F_{Anj}}{\Delta A_{nj}})^2 + (\frac{\Delta F_{\Phi nj}}{\Delta \Phi_{nj}})^2]}} \tag{21}$$

$$r_{\Phi nj} = \frac{\frac{\Delta F_{\Phi nj}}{\Delta \Phi_{nj}}}{\sqrt{\sum_{n=1}^{N}[(\frac{\Delta F_{Anj}}{\Delta A_{nj}})^2 + (\frac{\Delta F_{\Phi nj}}{\Delta \Phi_{nj}})^2]}} \quad . \tag{22}$$

The new amplitude and phase settings of the $(j+1)$th transmit-weight configuration are computed according to

$$A_{n,j+1} = A_{nj} + \Delta A_{nj} r_{Anj} \tag{23}$$

$$\Phi_{n,j+1} = \Phi_{nj} + \Delta \Phi_{nj} r_{\Phi nj} \quad . \tag{24}$$

For the current software implementation of the gradient search in these experiments, the step sizes are assumed (for convenience) to be independent of both the iteration number and the adaptive channel number, that is

$$\Delta A_{nj} = \Delta A \tag{25}$$

$$\Delta \Phi_{nj} = \Delta \Phi \quad . \tag{26}$$

In some situations it may be desirable to change the step size at each iteration as considered in Farina and Flam [73] and Hasdorff [72], but that possibility has not been explored in current measurements.

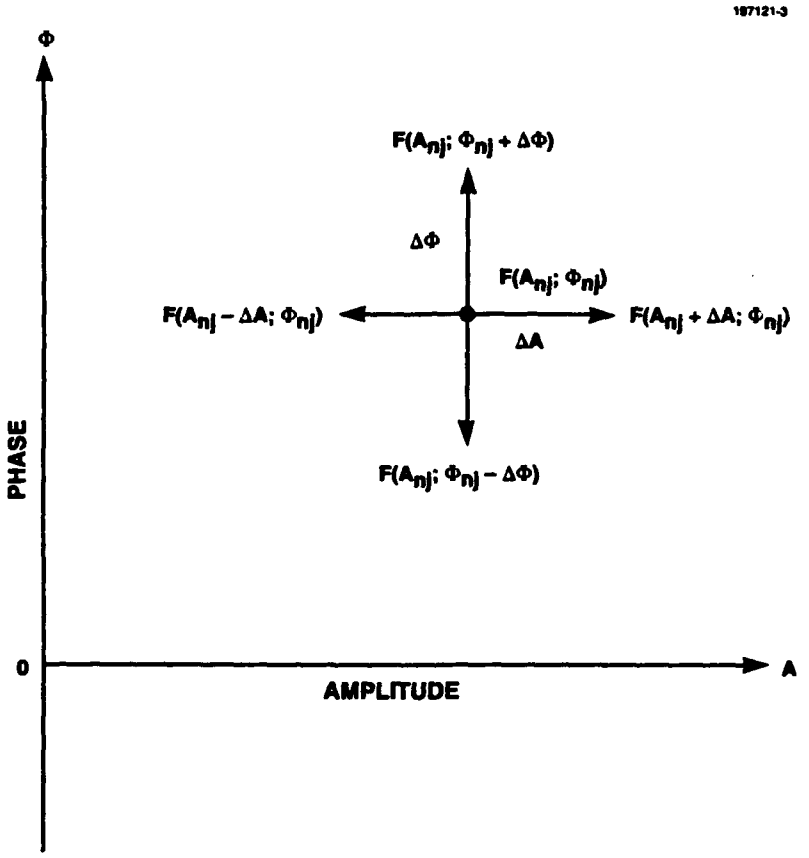

Figure 5. Figure of merit with transmit-weight dithering for optimum search directions.

2.3 System Considerations

Figure 6 is a block diagram of an adaptive hyperthermia system controlled by the gradient-search algorithm. Transmit weights $w_{1j}, \cdots, w_{nj}, \cdots, w_{Nj}$ at the jth iteration are shown at the top of the figure. The transmit phased-array antenna induces a voltage across the terminals of the ith receive field probe antenna. For any given configuration of the transmit weights, each weight is dithered by a small amount in amplitude and phase, and the received powers at the E-field probes are stored in the computer for calculation of f, search directions, and updated $(j+1)$th transmit-weight configuration. One transmit weight is dithered with the remaining transmit weights in their jth state. The figure of merit F_j in the adaptive hyperthermia system is the power received by the auxiliary probe array, as indicated in the block diagram. Search directions for the adaptive transmit weights are based on maximizing the auxiliary probe array received power and are computed based on Equations (21) and (22). Transmit weights for the next configuration $(j+1)$ are computed from Equations (23) and (24). The adaptive weight vector $\boldsymbol{w}_a$ is achieved when the $(j+1)$th weight configuration has converged. Based on other measurements [10,12] not shown here, convergence occurs typically in less than 20 iterations, depending on the step sizes (ΔA and $\Delta\Phi$).

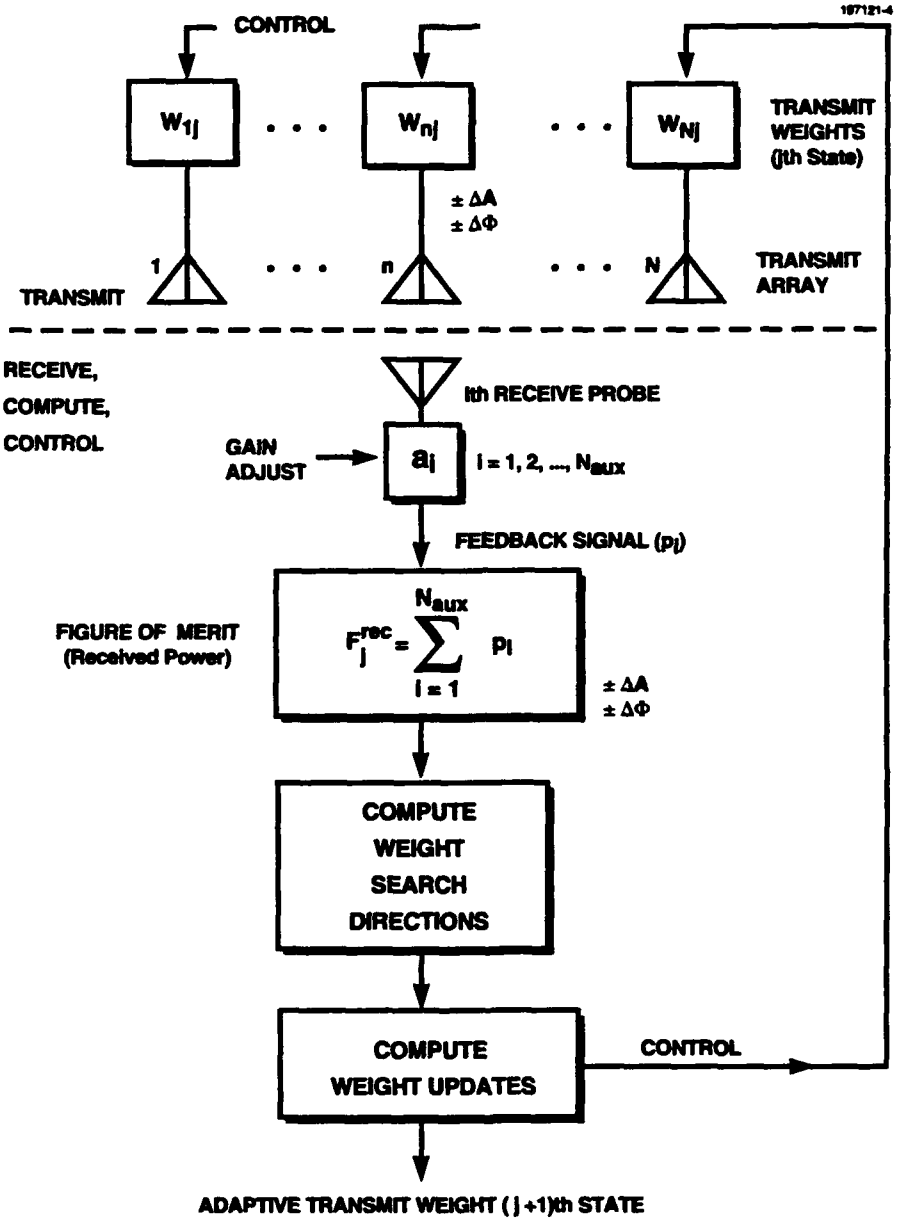

Figure 6. Gradient-search algorithm block diagram for adaptive focusing hyperthermia system.

3. MATERIALS AND METHODS

The hyperthermia phased-array system used in these measurements is the Labthermics Technologies Microtherm-1000 planar phased-array applicator (Figure 1), using a 15- × 15-cm planar array with a 4 × 4 grid of uniformly spaced square waveguide elements operating at 915 MHz (Figure 2). Figure 7 is a photograph of the planar phased-array applicator. Due to the water bolus covering the applicator, it is not possible to see the actual waveguide radiators of the array. The waveguide aperture dimensions are 3.8 × 3.8 cm, and the waveguides are loaded with a high-dielectric constant material to impedance-match the elements at 915 MHz. The waveguides are linearly polarized with the dominant E-field component aligned with the y-direction (refer to Figure 2). The variable transmit gain and phase modules are controlled by digital-to-analog (D/A) converters. There are 16 high-power amplifiers that drive the waveguides with up to 35-W average power per channel. The power applied to each element is controllable in 10% increments of the adjustable master power level. Each of the 16 active channels has an electronically controlled variable phase shifter (8 bits, 0° to 360°) for focusing the array. The phased-array applicator can be driven in incoherent mode (with 16 independently operating sources with frequencies near 915 MHz) or coherent mode (with a single frequency generator and independent control of the relative phase of each aperture to within 1.5°). Invasive Luxtron [78] fiber-optic temperature sensors are included with the Microtherm-1000 system to monitor the temperatures achieved during treatment.

The coupling bolus consists of deionized water contained within a flexible membrane, which can be expanded outward to 6 to 8 cm in front of the applicator face to possibly improve the microwave coupling to sharply contoured surfaces. Bolus temperature is controlled by circulating cooling water through a thermal conduction heat exchanger contained in the outer edges of the bolus housing. Cooling capacity and transient control of the coupling bolus in the UCSF Microtherm unit were improved by removing the plastic tubing heat exchanger inside the bolus and adding a closed-circuit pumping system to circulate temperature-controlled deionized water directly through the bolus compartment in series with a heat exchanger mounted in a temperature-regulated water bath. A cool water bolus between the patient and the phased array prevents excess heating of the skin surface. The bolus is filled with circulating deionized water, which has a very low microwave propagation loss.

The UCSF hyperthermia array (Figure 8) is controlled and monitored by an MS-DOS-based personal computer system, which implements the gradient-search adaptive focusing algorithm.

The E-field probe [59,60,62] used in these measurements was fabricated at UCSF and integrated with the Microtherm-1000 system. The E-field sensor is a 1.9-mm OD Schottky detector diode (HP-3486), operating in the square law region with the diode leads arranged to form a dipole antenna of 1-cm length. The sensor is coupled to an amplifier circuit (Figure 9) via high-resistance

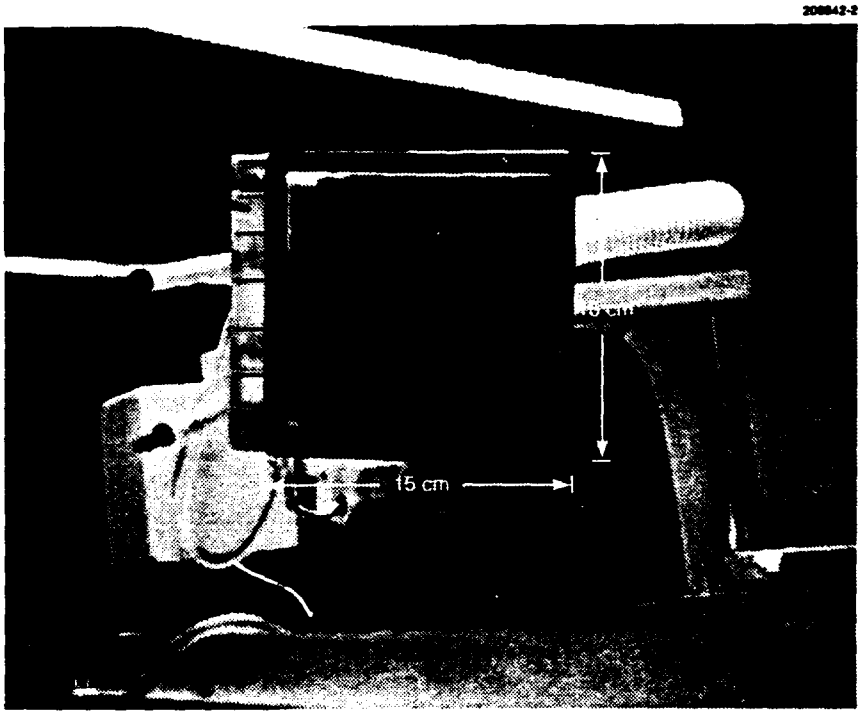

Figure 7. The 915-MHz microwave planar phased-array applicator used in the Labthermics Microtherm-1000 system.

lead material (60 kΩ/m)[2] to minimize perturbation of the fields. The rectified DC output voltage is a function of the E-field squared in the orientation of the dipole leads. The dipole probe hardware and probe (x, y, z) positioner are shown in Figure 10. A 12-bit analog-to-digital (A/D) converter samples the E-field probe signal.

A liquid-type (salt and sugar dissolved in deionized water) muscle-equivalent phantom was used (σ = 1.38 S/m, relative permittivity ϵ_r = 54.7 [79]), having electrical properties similar to high water content tissues at 915 MHz (ϵ_r = 51.0 and σ = 1.28 S/m [80]). The liquid phantom was placed within a 50- x 50- x 22-cm-deep Plexiglas tank (Figure 10).

[2]From Holaday Industries; 1.2-mm OD, including outer insulation.

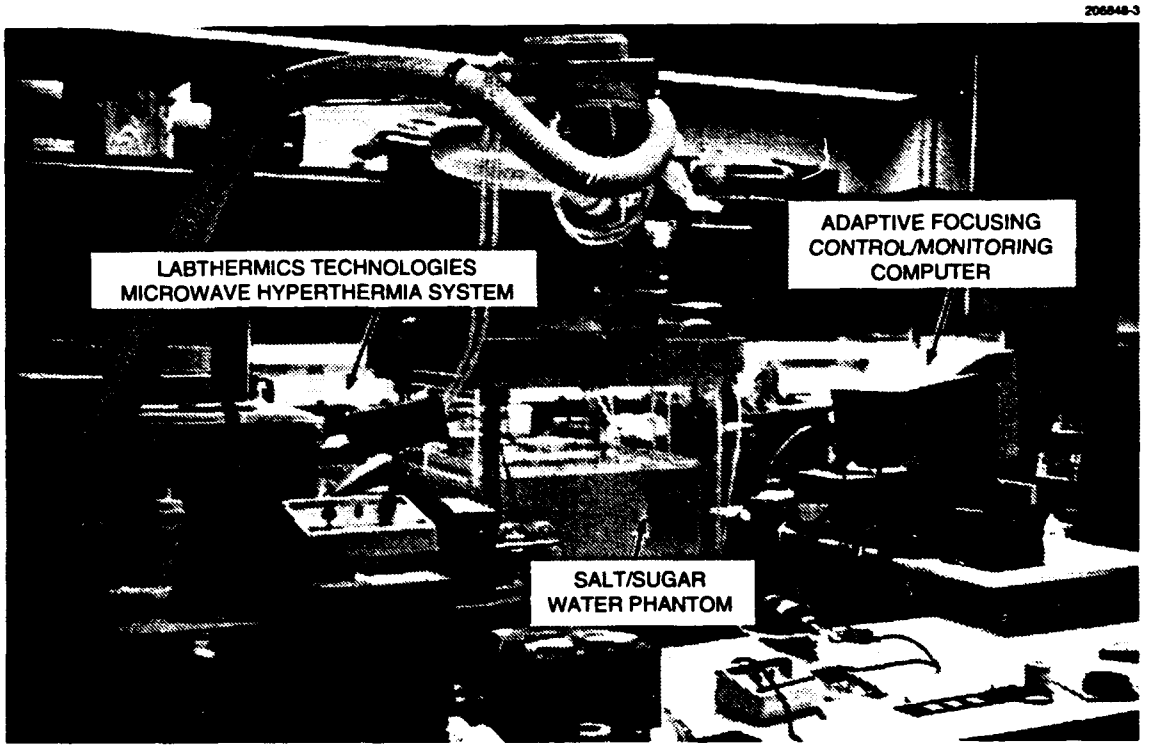

Figure 8. UCSF/MIT adaptive hyperthermia experiments equipment.

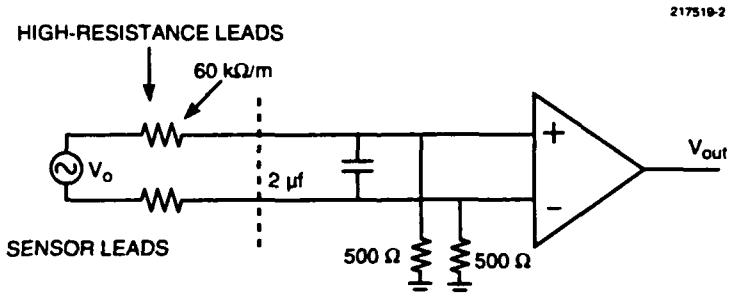

Figure 9. Amplifier circuit for E-field probe.

A computer program that implements the gradient-search algorithm was developed by MIT Lincoln Laboratory and integrated by UCSF with the Labthermics system. The MIT/UCSF integrated software allows the operator to run an adaptive focusing algorithm that uses the output power of the E-field probe as a feedback signal during the gradient search. The adaptive focusing algorithm uses only phase control to maximize the focal point E-field.

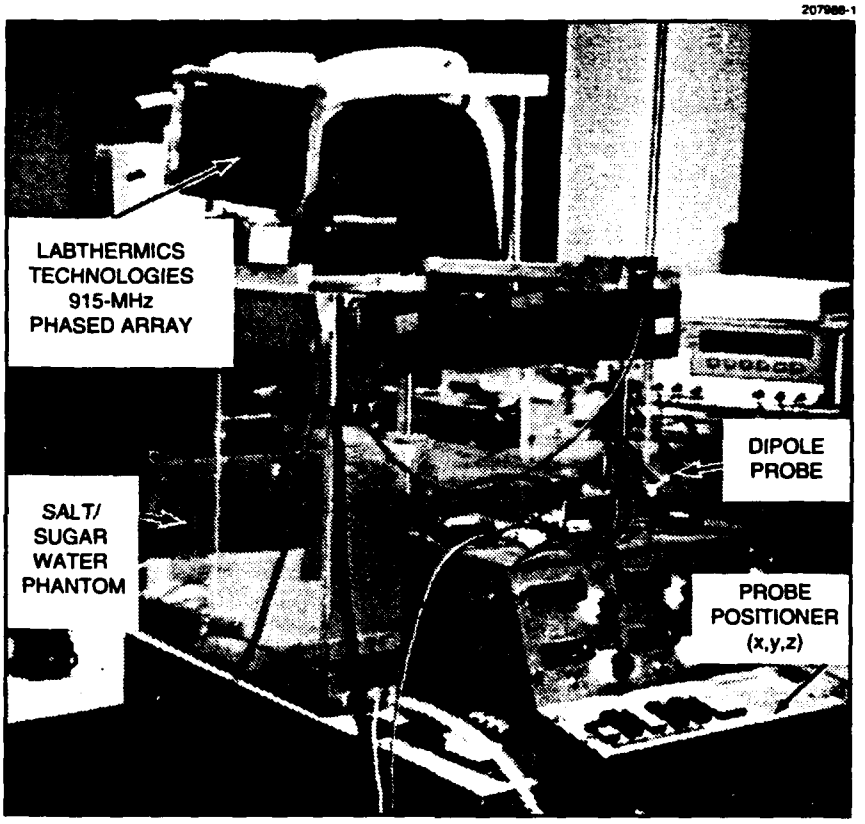

Figure 10. Dipole probe, probe (x, y, z) positioner system, and the muscle-equivalent phantom tank.

4. MEASURED RESULTS

4.1 Review of Earlier Investigations at UCSF

This section reviews data previously measured by UCSF that demonstrate several capabilities of the Labthermics system. At UCSF, initial efforts to study the electrical phasing capabilities of the Microtherm-1000 unit proved difficult due to irregular radiation beam profiles and magnitudes of individual waveguide apertures [81] and the inability to accurately calibrate or preset the individual phase shifters to absolute values. Attempts at using theoretically selected phases that were applied to each element were unsuccessful or produced marginal results in a water phantom. To compensate for these problems and to accommodate expected tissue heterogeneities in vivo, a phase selection or optimization scheme was developed to iteratively select the phasing of each transmit channel to maximize the measured SAR at the desired location. A computer/software system linked to the Microtherm unit turns on individual elements of the phased array in a predetermined sequence and iteratively adjusts the phasing until a maximum SAR is recorded. The next element in the sequence is turned on and phase-adjusted similarly to maximize the SAR. This phasing process continues until all elements are phase-focused. This phasing approach attempted to focus in deionized water, tissue-equivalent liquid phantoms, and in vivo pig thigh [58]. With the UCSF phasing scheme, it was possible to focus the Microtherm at depths of 7 cm in the deionized water phantom as shown in Figure 11(a). (The measured E-field radiation pattern contours in Figure 11 are given in 10% intervals.) Clearly, in the deionized water maximum radiation occurs in the vicinity of the desired focus. Based on the 50% SAR value, the maximum penetration depth is 15 cm in the deionized water medium. Using the same algorithm, similar focusing attempts in muscle-equivalent phantom [Figure 11(b)] did not generate a useful focused beam but produced, in essence, a collimated beam with a beam peak effectively at the surface of the phantom. The data in Figure 11(b) indicate a maximum penetration depth of 3 cm, based on the 50% contour that reaches $z = 3$ cm. (Microwave propagation loss in deionized water is 0.3 dB/cm, whereas in muscle-equivalent phantom, loss is close to 3 dB/cm.) Propagation loss in muscle tissue clearly contributes greatly to the inability to focus the 915-MHz planar phased array at the desired depth. Even with the degradation in focus, a 3-cm penetration depth is potentially useful for certain tumors.

The efficacy of the UCSF focusing algorithm was evaluated in a pig thigh model, where the phase was optimized using an implanted SAR sensor. Figure 12 shows the in vivo experimental set-up with trial focus positions ($z = 2.5$ and 4.5 cm) indicated by the shaded circles located on the central axis. In the incoherent mode with the 16 waveguides operating independently, the measured radiation pattern in Figure 13(a) indicates a maximum penetration depth of about 1 cm on the central axis, consistent with a microwave propagation loss of 3 dB/cm. Figures 13(b) and (c) show the measured radiation pattern for a focus at $z = 2.5$ and 4.5 cm, respectively. Focused at $z = 2.5$ cm [Figure 13(b)], the measured maximum penetration depth (on the principal axis) is 2.3 cm, and the beam peak is at $z = 1$ cm. Focused at $z = 4.5$ cm [Figure 13(c)], however, penetration depth is only 1.9 cm, and the beam peak is at the surface of the target. Intuitively, one would expect the $z = 4.5$-cm focus to penetrate deeper than the $z = 2.5$-cm focus. Instead, measurements indicate

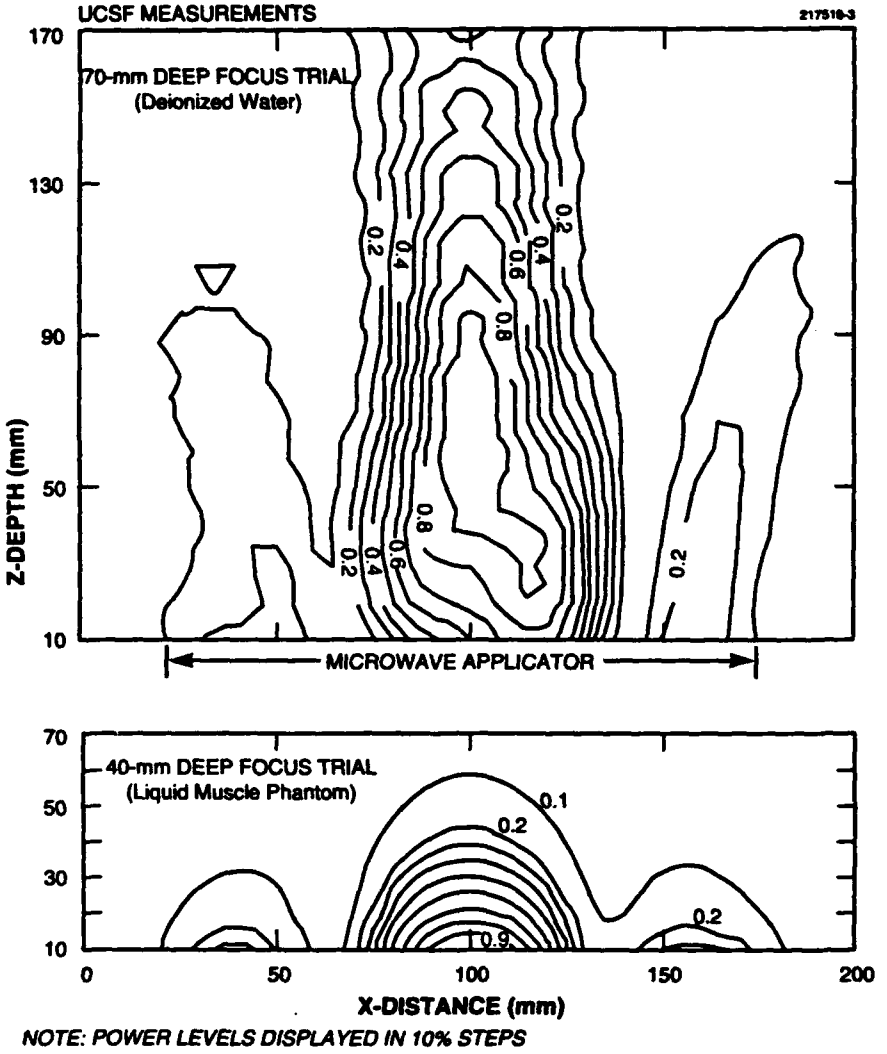

Figure 11. Measured E-field radiation pattern for Microtherm-1000 planar phased array focused at (a) z = 7 cm in deionized water phantom (propagation loss = 0.9 dB/cm), resulting in a well-focused beam; (b) z = 4 cm in muscle-equivalent liquid phantom (propagation loss = 9 dB/cm), resulting in a beam that is not centered at the desired focusing depth.

a reduction in penetration depth when the focus is increased beyond $z = 2.5$ cm. This discrepancy was the principal reason that UCSF was interested in comparing the MIT Lincoln Laboratory gradient-search algorithm with the systematic iterative-search algorithm currently used with the Microtherm system. Figure 14 compares the measured SAR[3] and temperature distributions for the $z = 2.5$-cm focus case, and the two sets of data are consistent; that is, the peak temperature value occurs near the peak of the SAR distribution.

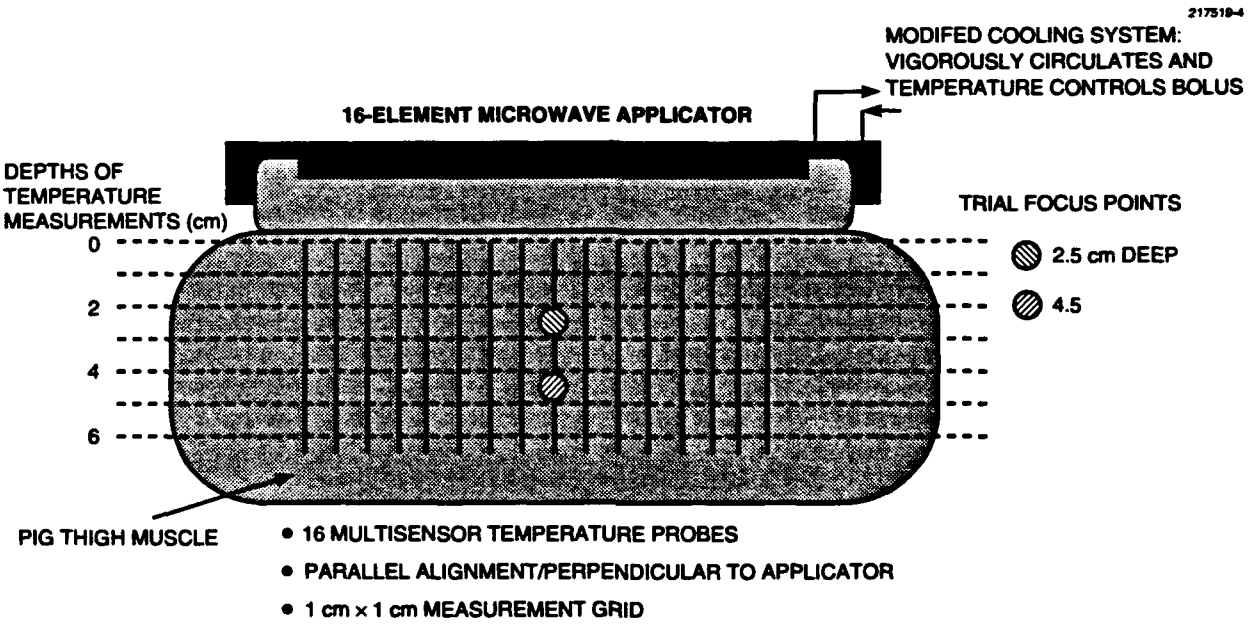

Figure 12. UCSF experimental test set-up for in vivo measurements of pig thigh.

From these measurements it is concluded that by optimizing the phasing of the Microtherm it is possible to focus in a low-loss deionized water phantom. The focused power depositions in muscle phantom and tissue do not produce a useful focus but illustrate a possible improvement in penetration depth. One question that remains concerns the validity of the UCSF optimization routine

---

[3]Defined here as SAR = $c\Delta T/\Delta t$ where ΔT is the change in temperature over time interval Δt and c is the specific heat.

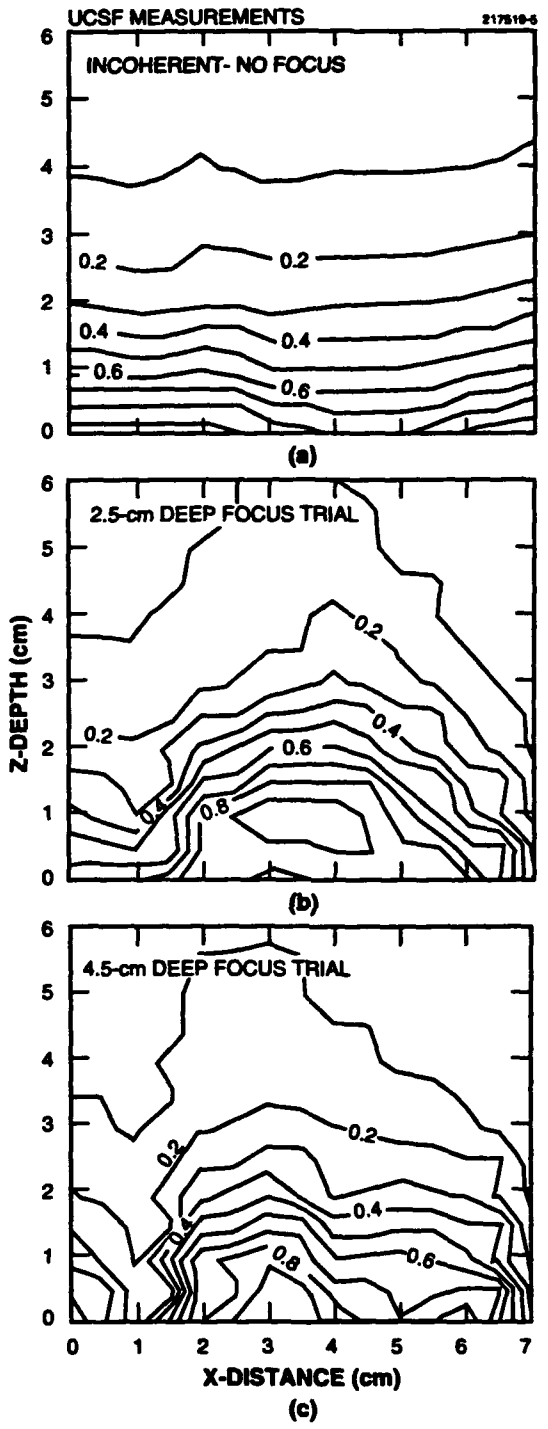

Figure 13. Measured E-field radiation pattern for Microtherm-1000 planar phased array illuminating muscle-equivalent liquid phantom (propagation loss = 9 dB/cm): (a) incoherent mode (all elements incoherently driven); focused at z = (b) 2.5 and (c) 4.5 cm.

and whether better focusing in a lossy medium could be obtained with an adaptive optimization algorithm as considered previously [7,10,12]. New measurements follow.

4.2 New Measurements at UCSF

UCSF and MIT Lincoln Laboratory began collaborating in June 1992 to implement an adaptive focusing, gradient-search algorithm with the Microtherm-1000. Experiments using the UCSF and MIT iterative-search algorithms were performed in the deionized water and the muscle-equivalent liquid phantoms. Phase focusing was attempted in the central axis of the Microtherm applicator at depths of 6 and 8 cm from the lowest ridge on the applicator housing with an additional 3-cm path length in deionized water from the apertures to this point. Measured E-field patterns (Figure 15) with the focus set at 8 cm indicate that both optimization schemes work similarly, producing well-defined focused beams at the desired depths. Current measurements have not considered field mapping in other vertical and horizontal planes that are necessary to characterize the locations and magnitudes of side- and possible grating lobes. It is interesting to note that the radiation patterns in Figure 15 exhibit a z-dependent ripple with spacing equal to $\approx$ 1.8 cm. This ripple is likely due to a standing-wave pattern created by incident and reflected waves in the phantom water tank. Assuming a dielectric constant of 80 and an electrical conductivity of 0.19 S/m, the wavelength of 915-MHz microwave radiation in deionized water is 3.6 cm. Thus the ripple spacing is equal to one-half wavelength as expected with a standing-wave pattern.

Measurements in the muscle-equivalent phantom were performed at a depth of 4 cm for three cases of amplitude illumination: equal applied at 100% of selected power level (Figure 16), adjusted uniform using premeasured SAR amplitudes for each element (Figure 17) [81], and inverse-tapered by applying double the power to the outer elements (Figure 18). These radiation pattern measurements were similar to those obtained in earlier published studies [58]. Notice that there are only minor differences between the three radiation patterns of Figures 16 to 18. It is likely that the four-element group at the center of the array is the dominant contributor to the radiation pattern shape. Shown last is the convergence of the method of steepest-ascent algorithm for the case of the 4-cm focal depth. Appendix A lists the raw A/D data for the measured E-field probe power in an experiment consisting of 15 iterations of the phase focusing steepest-ascent algorithm. The A/D converted data are changed to power in decibels by computing $10\log(p)$, where p is the value (measured power) of the A/D converter. The measured E-field at the focus as a function of iteration number is displayed in Figure 19. Focal-probe power increases by 17 dB over the 15 iterations with the data indicating convergence in about 7. [Note: The maximum step size given by Equation (26) is five D/A states at each iteration. Also, each iteration takes less than 1 min to execute, thus the array is automatically focused in less than 10 min.]

The results from these investigations indicate that the low number (16) of array antenna elements, high attenuation of the signal from outer elements, and irregular beam patterns of the individual elements dictate that the Microtherm unit cannot produce a well-defined focus at any appreciable depth beyond 3 cm in lossy muscle tissue. Beam shaping and possible improvement in

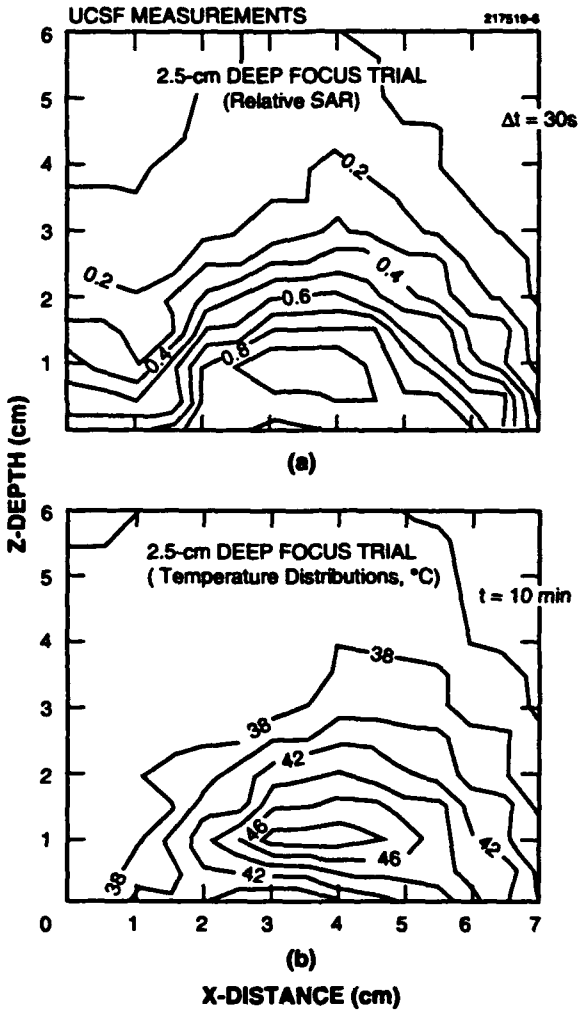

Figure 14. Comparison of (a) measured SAR and (b) temperature distributions (steady state, 10 min) for Microtherm-1000 system focused at 2.5 cm in pig thigh.

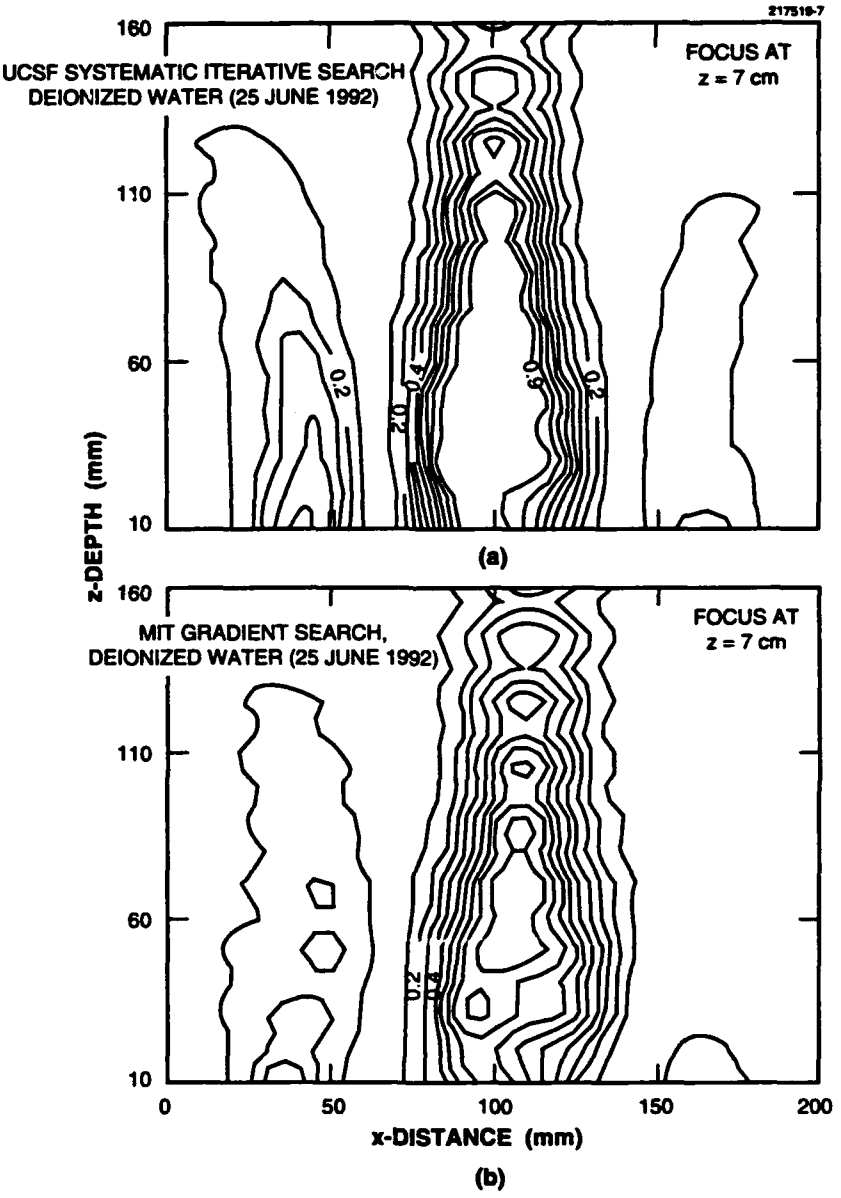

Figure 15. Comparison of measured two-dimensional radiation patterns of the Microtherm-1000 with focal depth of 8 cm in deionized water phantom: (a) UCSF systematic iterative-search focusing algorithm and (b) MIT Lincoln Laboratory adaptive gradient-search focusing algorithm.

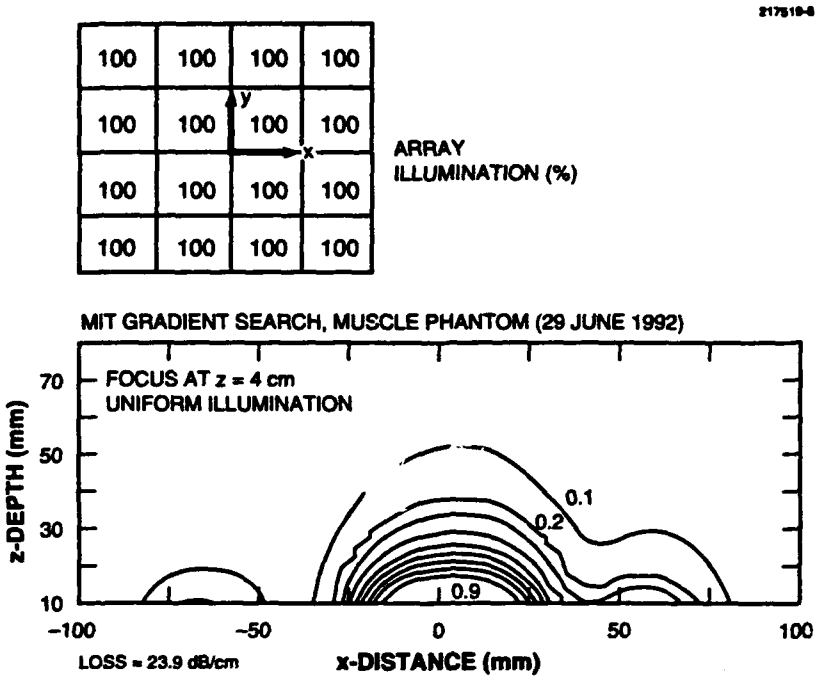

Figure 16. Measured two-dimensional radiation pattern of the Microtherm-1000 using MIT Lincoln Laboratory adaptive focusing algorithm with focal depth of 4 cm in muscle-equivalent liquid phantom. Power level of each waveguide is at 100% relative to each other (uniform illumination).

penetration depth with different illumination strategies is one aspect that can be studied, but significant improvement is not expected. Curved phased-array applicators with the radiating antenna elements pointed toward the focus may improve effective penetration depth and will be investigated in future measurements. Because two proven types of phase optimization routines yield similar results, confidence exists that the measured data truly depict the best possible performance of the Microtherm system.

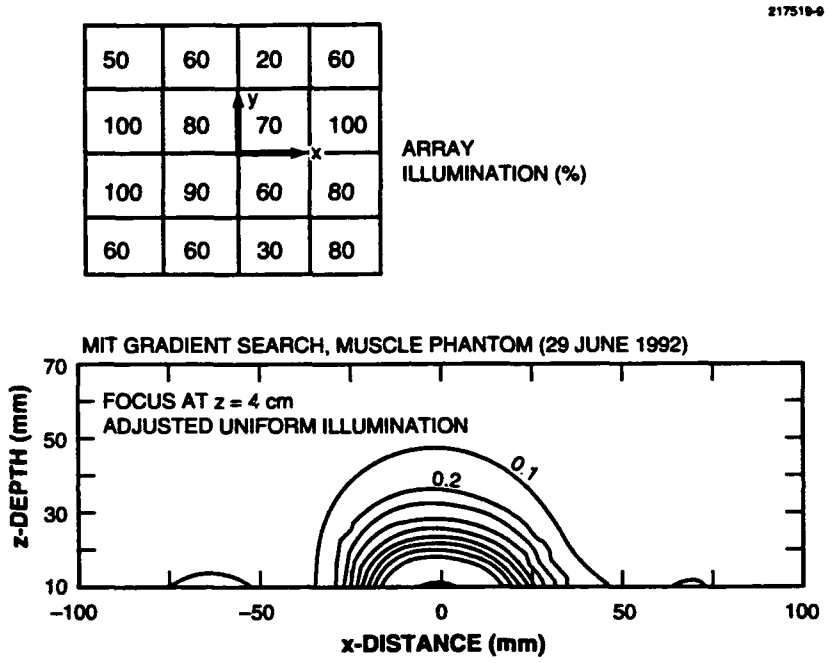

Figure 17. Measured two-dimensional radiation pattern of the Microtherm-1000 using MIT Lincoln Laboratory adaptive focusing algorithm with focal depth of 4 cm in muscle-equivalent liquid phantom. Power level of each waveguide is adjusted to provide equal amplitude as measured at the focusing probe (adjusted uniform illumination).

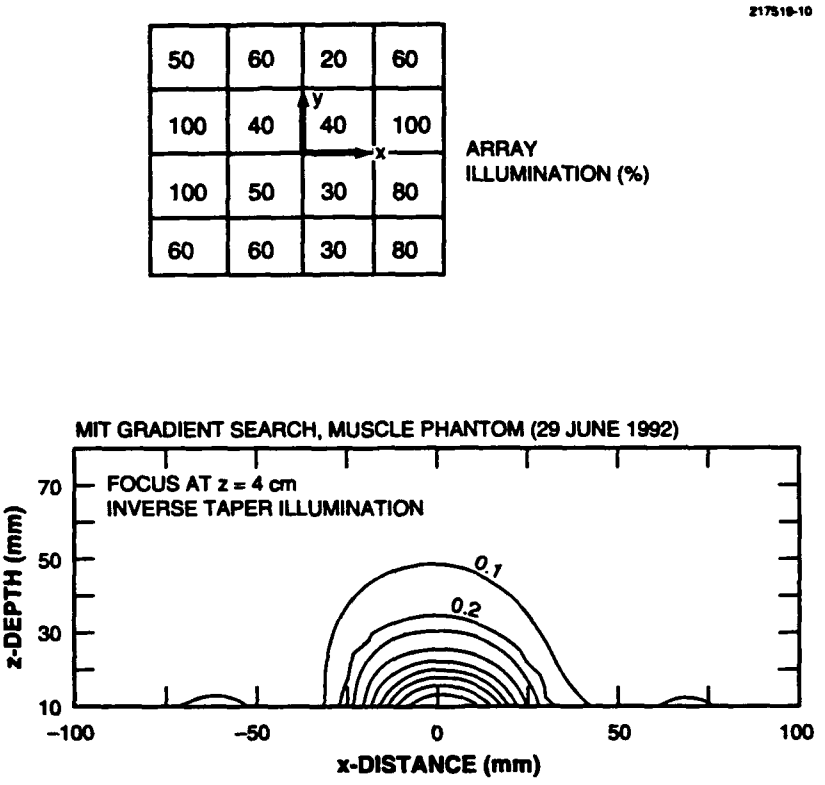

Figure 18. Measured two-dimensional radiation pattern of the Microtherm-1000 using MIT Lincoln Laboratory adaptive focusing algorithm with focal depth of 4 cm in muscle-equivalent liquid phantom. Power level of the outer ring of waveguides is adjusted to provide twice the power of the inner ring of elements as measured at the focusing probe (inverse taper illumination).

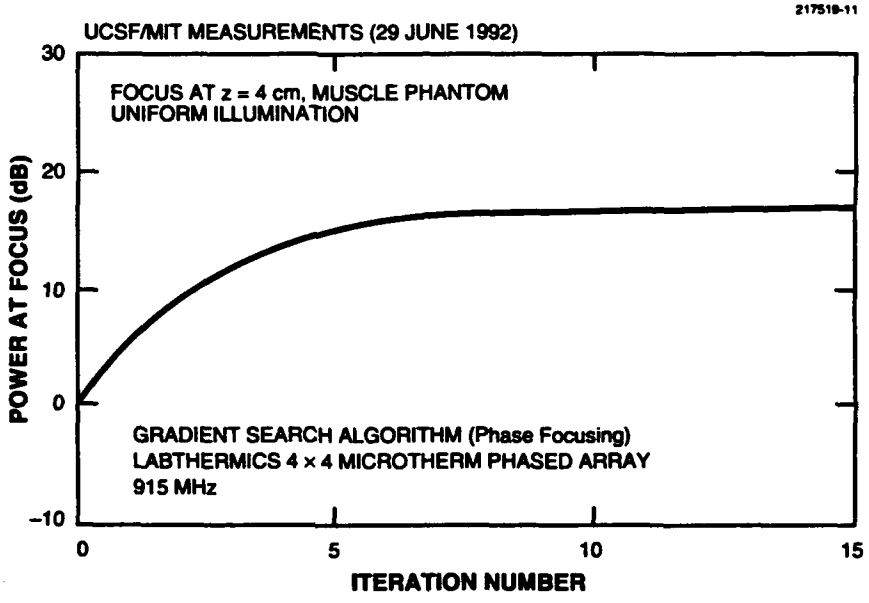

Figure 19. Measured E-field focused at z = 4 cm as a function of adaptive phase focusing gradient-search iteration number for a muscle-equivalent liquid phantom. Power level at the focus increases by 17 dB due to the adaptive gradient search.

5. CONCLUSION

An adaptive focusing, 915-MHz, microwave planar phased-array hyperthermia system has been experimentally demonstrated by modifying a commercial version at the University of California at San Francisco. The measurements shown in this report demonstrate that the E-field radiation pattern of a hyperthermia planar phased array can be controlled by an adaptive feedback gradient-search focusing algorithm. E-field focusing (power maximization) at a desired phantom target position has been experimentally demonstrated.

In this report, the adaptive algorithm is a gradient-search feedback technique (method of steepest ascent) derived in Section 2. The gradient search employs transmit-weight phase dithering with E-field probe power measurements at the desired target position to calculate the required gradient-search directions for microwave focusing. The steepest ascent algorithm produces two-dimensional radiation patterns that are similar to those produced by a systematic iterative focusing algorithm previously demonstrated with measurements at UCSF.

E-field focusing is intended to maximize the microwave power delivered to a tumor site. The data presented in this report suggest that this goal may be achieved for shallow tumors (less than 3 cm beneath the skin surface) with an adaptive focusing, hyperthermia microwave planar phased-array system. Measurements have proven that a planar phased array at 915 MHz can only provide a useful focus in lossy (3 dB/cm) muscle tissue at a maximum depth of 3 cm.

Because of the hard- and software modifications made at UCSF, the 16-channel 915-MHz Microtherm-1000 system can serve as a test bed for new types of adaptive phased-array applicators. For example, it may be possible to generate a focus deeper than 3 cm with a curved phased-array geometry because radiating antennas on a curved contour tend to have peak radiation toward the focus and propagation path length between the antennas and the focus will vary slightly from element to element. Thus the curved (compared with the planar) array may provide a better focus at depth. Future measurements will investigate a new noninvasive, monopole, adaptive phased-array, 915-MHz microwave applicator (recently designed and fabricated at MIT Lincoln Laboratory) with other types as they become available.

APPENDIX A
Measured E-Field Probe Raw Data

Measured Raw A/D Converter Data for E-Field Probe at Focus

Adaptive Focus, Muscle-Equivalent Liquid Phantom

Focus at z = 4 cm of Phantom (run wfa8x), Method of Steepest-Ascent Algorithm

j = iteration number
P1 = probe 1 (tumor site)

j	P1
0	1.2
1	4.6
2	10.1
3	18.5
4	27.0
5	35.4
6	42.6
7	48.5
8	52.8
9	55.8
10	57.9
11	58.8
12	61.1
13	62.2
14	62.8
15	64.2

Note: The above A/D measured data are converted to decibels by taking 10 times the log of the tabulated numbers.

REFERENCES

1. M.I. Skolnik, *Introduction to Radar Systems*, 2nd ed., New York: McGraw-Hill Book Company (1980).

2. R.T. Compton, Jr., *Adaptive Antennas, Concepts and Performance*, Englewood Cliffs, N.J.: Prentice Hall (1988).

3. A. Farina, *Antenna-based signal processing techniques for radar systems*, Norwood, Mass.: Artech House (1992).

4. R. Nitzberg, *Adaptive signal processing for radar*, Norwood, Mass.: Artech House (1992).

5. A.J. Fenn, "Application of adaptive nulling to electromagnetic hyperthermia for improved thermal dose distribution in cancer therapy," Lexington, Mass.: MIT Lincoln Laboratory (3 July 1991), DTIC AD-A241026.

6. A.J. Fenn, "Focused near-field nulling for adaptive electromagnetic hyperthermia applications," *1991 Prog. Electromagn. Res. Symp. Proc.* (1–5 July 1991), p. 393.

7. A.J. Fenn, "Adaptive hyperthermia for improved thermal dose distribution," in J.D. Chapman, W.C. Dewey, and G.F. Whitmore, eds., *Radiation Research: A Twentieth-Century Perspective* I*: Congress Abstracts, 7–12 July 1991*, San Diego, Calif.: Academic Press, Inc. (1991), p. 290.

8. A.J. Fenn, "Noninvasive adaptive nulling for improved hyperthermia thermal dose distribution," *IEEE Eng. Medicine Biol. Soc. Int. Conf.* **13**, 976–977 (31 October–3 November 1991).

9. A.J. Fenn and G.A. King, "An adaptive radio-frequency hyperthermia phased-array system for improved cancer therapy: Phantom target measurements," Lexington, Mass.: MIT Lincoln Laboratory, Project Report ACC-3 (April 1992).

10. G.A. King and A.J. Fenn, "Adaptive nulling measurements with the BSD Sigma-60 applicator for improved hyperthermia thermal distribution," *Sixth Int. Congress on Hyperthermic Oncol.* (26 April–1 May 1992).

11. A.J. Fenn and G.A. King, "Adaptive nulling in the hyperthermia treatment of cancer," *Linc. Lab. J.* **5**, 223–240 (1992).

12. A.J. Fenn and G.A. King, "An adaptive radio-frequency hyperthermia phased-array system for improved cancer therapy: Phantom target measurements," Submitted to *Int. J. Hyperthermia.*

13. P.F. Turner, T. Schaefermeyer, and T. Saxton, "Future trends in heating technology of deep-seated tumors," *Recent Results in Cancer Res.* **107**, 249–262 (1988).

14. P.F. Turner, A. Tumeh, and T. Schaefermeyer, "BSD-2000 approach for deep local and regional hyperthermia: Physics and technology," *Strahlentherapie Onkologie* **165**, 738–741 (1989).

REFERENCES
(Continued)

15. C.A. Perez and L.W. Brady, *Principles and Practice of Radiation Oncology.* Philadelphia, Penna.: J.B. Lippincott Co. (1987).

16. A.W. Guy, "History of biological effects and medical applications of microwave energy," *IEEE Trans. Microw. Theory Tech.* **MTT-32**, 1182–1200 (September 1984).

17. J. Overgaard, "The effect of local hyperthermia alone and in combination with radiation on solid tumors," in C. Streffer, ed., *Cancer Therapy by Hyperthermia and Radiation, Proc. 2nd Int. Symp.*, Baltimore, Md.: Urban & Schwarzenberg, Inc. 49–61 (1978).

18. J. Overgaard, "Clinical hyperthermia, an update," *Proc. 8th Int. Congress Radiation Res.* **2**, 942–947 (July 1987).

19. S.B. Field and J.W. Hand, eds., *An Introduction to the Practical Aspects of Clinical Hyperthermia*, London: Taylor & Francis (1990).

20. "Special issue on cancer therapy by electromagnetic hyperthermia," *J. Microw. Power* **16** (June 1981).

21. "Special issue on phased arrays for hyperthermia treatment of cancer," *IEEE Trans. Microw. Theory Tech.* **MTT-34** (May 1986).

22. "Special issue on hyperthermia and cancer therapy," *IEEE Trans. Biomed. Eng.* **BME-31** (January 1984).

23. V. Sathiaseelan, M.F. Iskander, G.C.W. Howard, and N.M. Bleehen, "Theoretical analysis and clinical demonstration of the effect of power control using the annular phased-array hyperthermia system," *IEEE Trans. Microw. Theory Tech.* **MTT-34** 514–519 (May 1986).

24. V. Sathiaseelan, "Potential for patient-specific optimization of deep heating patterns through manipulation of amplitude and phase," *Strahlentherapie Onkologie* **165** 743–745 (1989).

25. D. Sullivan, "Three-dimensional computer simulation in deep regional hyperthermia using the finite-difference time-domain method," *IEEE Trans. Microw. Theory Tech.* **MTT-38** 204–211 (February 1990).

26. B.S. Trembly, A.H. Wilson, M.J. Sullivan, A.D. Stein, T.Z. Wong, and J.W. Strohbehn, "Control of the SAR pattern within an interstitial microwave array through variation of antenna driving phase," *IEEE Trans. Microw. Theory Tech.* **MTT-34** 568–571 (May 1986).

27. G. Sato, C. Shibata, S. Sekimukai, H. Wakabayashi, K. Mitsuka, and K. Giga, "Phase-controlled circular array heating equipment for deep-seated tumors: Preliminary experiments," *IEEE Trans. Microw. Theory Tech.* **MTT-34** 520–525 (May 1986).

REFERENCES
(Continued)

28. P.A. Cudd, A.P. Anderson, M.S. Hawley, and J. Conway, "Phased-array design considerations for deep hyperthermia through layered tissue," *IEEE Trans. Microw. Theory Tech.* **MTT-34** 526–531 (May 1986).

29. N. Morita, T. Hamasaki, and N. Kumagai, "An optimal excitation method in multiapplicator systems for forming a hot zone inside the human body," *IEEE Trans. Microw. Theory Tech.* **MTT-34** 532–538 (May 1986).

30. C. De Wagter, "Optimization of simulated two-dimensional temperature distributions induced by multiple electromagnetic applicators," *IEEE Trans. Microw. Theory Tech.* **MTT-34** 589–596 (May 1986).

31. M. Knudsen and U. Hartmann, "Optimal temperature control with phased-array hyperthermia system," *IEEE Trans. Microw. Theory Tech.* **MTT-34** 597–603 (May 1986).

32. C.F. Babbs, V.A. Vaguine, and J.T. Jones, "A predictive-adaptive, multipoint feedback controller for local heat therapy of solid tumors," *IEEE Trans. Microw. Theory Tech.* **MTT-34** 604–611 (May 1986).

33. R.B. Roemer, "Physical and engineering aspects of hyperthermia," *Proc. 8th Int. Congress Radiation Res.* **2** 948–953 (July 1987).

34. R.B. Roemer, K. Hynynen, C. Johnson, and R. Kress, "Feedback control and optimization of hyperthermia heating patterns: Present status and future needs," *IEEE Eighth Annual Conf. Eng. Med. Biol. Soc.*, 1496–1499 (November 1986).

35. R.B. Roemer, "Optimal power deposition in hyperthermia. I. The treatment goal: The ideal temperature distribution: The role of large blood vessels," *Int. J. Hyperthermia* **7** 317–341 (March–April 1991).

36. A. Boag and Y. Leviatan, "Optimal excitation of multiapplicator systems for deep regional hyperthermia," *IEEE Trans. Biomed. Eng.* **BME-37** 987–995 (October 1990).

37. P. Wust, J. Nadobny, R. Felix, P. Deuflhard, A. Louis, and W. John, "Strategies for optimized application of annular-phased-array systems in clinical hyperthermia," *Int. J. Hyperthermia* **7** 157–173 (January–February 1991).

38. D.B. Nguyen and J.W. Strohbehn, "Optimal positions, orientations, amplitudes and phases of movable microwave applicators in hyperthermia treatment," in T. Sugahara and M. Saito, eds., *Hyperthermic Oncol. 1988* **1**, London: Taylor & Francis, 738–739 (1989).

39. J.W. Strohbehn, E.H. Curtis, K.D. Paulsen, and D.R. Lynch, "Optimization of the absorbed power distribution for an annular phased-array hyperthermia system," *Int. J. Radiation Oncol. Biol. Phys.*, 589–599 (1989).

REFERENCES
(Continued)

40. J.T. Loane III and S.W. Lee, "Gain optimization of a near-field focusing array for hyperthermia applications," *IEEE Trans. Microw. Theory Tech.* MTT-37 1629–1635 (October 1989).

41. E.S. Ebbini, H. Wang, M. O'Donnell, and C.A. Cain, "Acoustic feedback for hyperthermia phased-array applicators: Aberration correction, motion compensation, and multiple focusing in the presence of tissue inhomogeneities," *Proc. IEEE 1991 Ultrason. Symp.* 2 1343-1346 (1991).

42. E.S. Ebbini and C.A. Cain, "Experimental evaluation of a prototype cylindrical section ultrasound hyperthermia phased-array applicator," *IEEE Trans. Ultrason. Ferroelectr. Freq. Control* 38 510–520 (1991).

43. E.S. Ebbini and C.A. Cain, "Multiple-focus ultrasound phased-array pattern synthesis: Optimal driving signal distributions for hyperthermia," *IEEE Trans. Ultrason. Ferroelectr. Freq. Control* 36 540-548 (1989).

44. G.H. Nussbaum, "Quality assessment and assurance in clinical hyperthermia: Requirements and procedures," *Cancer Res. (Suppl.)*, 44:4811s–4817s (1984).

45. D.L. Denman, M.J. Kolasa, H.R. Elson, B.S. Aron, and J.G. Kereikes, "Specific absorption rates in simulated tissue media for a 10 × 10 cm 915-MHz waveguide applicator," *Med. Phys.* 14 681–686 (1987).

46. C.K. Chou, J.A. McDougall, K.W. Chan, and K.H. Luk, "Evaluation of captive bolus applicators," *Med. Phys.* 17 705–709 (1990).

47. W.L. Straube, R.J. Myerson, B. Emami, and L.B. Leybovich, "SAR patterns of external 915-MHz microwave applicators," *Int. J. Hyperthermia* 6 665–670 (1990).

48. P. Fessenden, D.S. Kapp, E.R. Lee, and T.V. Samulski, "Clinical microwave applicator design," in B.R. Paliwa , F.W. Hetzel, and M.W. Dewhirst, eds., *Biological, physical and clinical aspects of hyperthermia, Medical Physics Monograph 16*, New York: American Institute of Physics, pp. 123–131 (1988).

49. C.A. Perez, B. Gillespie, T. Pajak, N. Hornback, B. Emami, and P. Rubin, "Quality assurance problems in clinical hyperthermia and its impact on therapeutic outcome: A report by the Radiation Therapy Oncology Group," *Int. J. Radiation Oncol. Biol. Phys.* 16 551 (1989).

50. M.D. Sherar, D.J. Newcombe, W.B. Taylor, and J.W. Hunt, "Investigation of heating patterns of the MA-100 and MA-120 microwave applicators under different water bolus arrangements at 915 MHz," in J.D. Chapman, W.C. Dewey, and G.F. Whitmore, eds., *Radiation Research: A Twentieth-Century Perspective* I*: Congress Abstracts, 7-12 July 1991*, San Diego, Calif.: Academic Press, Inc., p. 194 (1991).

REFERENCES
(Continued)

51. T.V. Samulski, P. Fessenden, E.R. Lee, D.S. Kapp, E. Tanabe, and A. McEuen, "Spiral microstrip hyperthermia applicators: Technical design and clinical performance," *Int. J. Radiation Oncol. Biol. Phys.* **18** 233–242 (1990).

52. A. Tennant, J. Conway, and A.P. Anderson, "A robot-controlled microwave antenna system for uniform hyperthermia treatment of superficial tumors with arbitrary shape," *Int. J. Hyperthermia* **6** 193–202 (1990).

53. M.K. Ghopal, J.W. Hand, M.L.D. Lumori, S. Alkhairi, K.D. Paulsen, and T.C. Cetas, "Current sheet applicator arrays for superficial hyperthermia of chest wall lesions," *Int. J. Hyperthermia* **8** 227–240 (1992).

54. H.R. Underwood, A.F. Peterson, and R.L. Magin, "Electric-field distribution near rectangular microstrip radiators for hyperthermia heating: Theory versus experiment in water," *IEEE Trans. Biomed. Eng.* **39** 146–153 (1992).

55. E.R. Lee, T.R. Wilsey, P. Tarczy-Hornoch, D.S. Kapp, P. Fessenden, A. Lohrbach, and S. Prionas, "Body conformable 915-MHz microstrip array applicators for large surface area hyperthermia," *IEEE Trans. Biomed. Eng.* **39** 470–483 (1992).

56. D.S. Kapp, P. Fessenden, T.V. Samulski, M.A. Bagshaw, R.S. Cox, E.R. Lee, A.W. Lohrbach, J.L. Meyer, and S.D. Prionas, "Stanford University Institutional Report. Phase I evaluation of equipment for hyperthermia treatment of cancer," *Int. J. Hyperthermia* **4** 75–115 (1988).

57. J.W. Hand, J.L. Cheetham, and A.J. Hind, "Absorbed power distributions from coherent microwave arrays for localized hyperthermia," *IEEE Trans. Microw. Theory Tech.* **34** 484–489 (1986).

58. C.J. Diederich, G. Sherwin, C. Adams, and P.R. Stauffer, "Evaluation of a multi-element microwave applicator for hyperthermia," in J.D. Chapman, W.C. Dewey, and G.F. Whitmore, eds., *Radiation Research: A Twentieth-Century Perspective, Volume I: Congress Abstracts, 7–12 July 1991*, San Diego, Calif.: Academic Press, Inc. p. 194 (1991).

59. H.I. Bassen, M. Swicord, and J. Abita, "A miniature broad-band electric field probe," *Annals of the New York Academy of Sciences, Biological Effects of Nonionizing Radiation* **247** 481–493 (1975).

60. H.I. Bassen and G.S. Smith, "Electric Field Probes—A Review," *IEEE Trans. Antennas Propag.* **AP-31** 710–718 (September 1983).

61. A. Uhlir, "Characterization of crystal diodes for low-level microwave detection," *Microw. J.* 59–67 (July 1963).

REFERENCES
(Continued)

62. C.H. Durney and M.F. Iskander, "Antennas for medical applications," in Y.T. Lo and S.W. Lee, eds., *Antenna Handbook: Theory, Applications, and Design*, New York: Van Nostrand Reinhold (1988).

63. A.J. Fenn, "Theory and analysis of near-field adaptive nulling," *1986 IEEE Antennas Propag. Soc. Int. Symp. Digest* **2**, New York: IEEE, 579–582 (1986).

64. A.J. Fenn, "Theory and analysis of near-field adaptive nulling," *1986 Asilomar Conf. on Signals, Systems and Computers*, Washington, D.C.: Computer Society Press of the IEEE, 105–109 (1986).

65. A.J. Fenn, "Theoretical near-field clutter and interference cancellation for an adaptive phased-array antenna," *1987 IEEE Antennas Propag. So. Int. Symp. Digest*, **1**, New York: IEEE, 46–49 (1987).

66. A.J. Fenn, "Moment-method analysis of near-field adaptive nulling," *IEEE Sixth Int. Conf. Antennas Propag., ICAP 89*, 295–301 (4–7 April 1989).

67. A.J. Fenn, "Evaluation of adaptive phased-array antenna far-field nulling performance in the near-field region," *IEEE Trans. Antennas Propag.* **38**, 173–185 (February 1990).

68. A.J. Fenn, "Near-field testing of adaptive radar systems," *Proc. 12th Annual Antenna Measurement Techniques Association Meeting and Symposium*, 13-9–13-14 (8–11 October 1990).

69. A.J. Fenn, H.M. Aumann, F.G. Willwerth, and J.R. Johnson, "Focused near-field adaptive nulling: Experimental investigation," *1990 IEEE Antennas Propag. Soc. Int. Symp. Digest* **1**, 186–189 (7–11 May 1990).

70. A.J. Fenn, "Analysis of phase-focused near-field testing for multiphase-center adaptive radar systems," *IEEE Trans. Antennas Propag.* **40**, 878–887 (August 1992).

71. R.L. Zahradnik, *Theory and Techniques of Optimization for Practicing Engineers*, New York: Barnes and Noble (1971), pp. 118–124.

72. L. Hasdorff, *Gradient Optimization and Nonlinear Control*, New York: John Wiley & Sons (1976).

73. D.J. Farina and R.P. Flam, "A self-normalizing gradient-search adaptive array algorithm," *IEEE Trans. Aerosp. Electron. Syst.* **27**, 901–905 (November 1991).

74. A. Cantoni, "Application of orthogonal perturbation sequences to adaptive beamforming," *IEEE Trans. Antennas Propag.* **AP-28**, 191–202 (March 1980).

75. L.C. Godara and A. Cantoni, "Analysis of the performance of adaptive beamforming using perturbation sequences," *IEEE Trans. Antennas Propag.* **AP-31**, 268–279 (March 1983).

REFERENCES
(Continued)

76. D.C. Farden and R.M. Davis, "Orthogonal weight perturbation algorithms in partially adaptive arrays," *IEEE Trans. Antennas Propag.* **AP-33**, 56–63 (January 1985).

77. A.J. Fenn, "Maximizing jammer effectiveness for evaluating the performance of adaptive nulling array antennas," *IEEE Trans. Antennas Propag.* **AP-33**, 1131–1142 (October 1985).

78. T.V. Samulski and E.R. Lee, "Preclinical evaluation of Luxtron 3000 system," *IEEE Eighth Annual Conf. Eng. in Medicine and Biol. Soc.*, 1493-1495 (1986).

79. G. Hartsgrove, A. Kraszewski, and A. Surowiec, "Simulated biological materials for electromagnetic radiation absorption studies," *Bioloelectromagnetics* **8**, 29–36, (1987).

80. J.W. Hand, "Biophysics and technology of electromagnetic hyperthermia," in M. Gautherie, ed., *Methods of External Hyperthermic Heating*, Berlin: Springer-Verlag (1990), pp. 1–59.

81. C.J. Diederich and P.R. Stauffer, "Pre-clinical evaluation of a microwave planar array applicator for superficial hyperthermia," *Int. J. Hyperthermia.* **9**, 227–246 (1993).

REPORT DOCUMENTATION PAGE

Form Approved
OMB No. 0704-0188

1. AGENCY USE ONLY (*Leave blank*)	2. REPORT DATE	3. REPORT TYPE AND DATES COVERED
	17 May 1993	Technical Report

4. TITLE AND SUBTITLE

Experimental Evaluation of an Adaptive Focusing Algorithm for a Microwave Planar Phased-Array Hyperthermia System at UCSF

5. FUNDING NUMBERS

C — F19628-90-C-0002
PE — 33110F, 33603F, 63226E
PR — 370

6. AUTHOR(S)

Alan J. Fenn, Chris J. Diederich, and Paul R. Stauffer

7. PERFORMING ORGANIZATION NAME(S) AND ADDRESS(ES)

Lincoln Laboratory, MIT
P.O. Box 73
Lexington, MA 02173-9108

8. PERFORMING ORGANIZATION REPORT NUMBER

TR-977

9. SPONSORING/MONITORING AGENCY NAME(S) AND ADDRESS(ES)

HQ Electronic Systems Center/ENK (AFMC)
Hanscom AFB
Bedford, MA 01731-5000

10. SPONSORING/MONITORING AGENCY REPORT NUMBER

ESC-TR-92-203

11. SUPPLEMENTARY NOTES

12a. DISTRIBUTION/AVAILABILITY STATEMENT

Approved for public release; distribution is unlimited.

12b. DISTRIBUTION CODE

13. ABSTRACT (*Maximum 200 words*)

An adaptive focusing microwave planar phased-array hyperthermia system for improved heating of superficial tumors is experimentally investigated. A commercial microwave hyperthermia planar phased-array antenna system at the University of California at San Francisco (UCSF) Radiation Oncology Department has been modified to implement a gradient-search adaptive focusing algorithm. Adaptive focusing measurements in a muscle-equivalent liquid phantom with a 915-MHz microwave planar phased-array hyperthermia system comprising 16 independent amplitude/phase-controlled waveguide antenna elements (Microtherm-1000, Labthermics Technologies, Inc.) are reported. An electric-(E-)field feedback probe detector, fabricated at UCSF, measures the E-field generated by the hyperthermia phased array. A method of steepest-ascent gradient-search feedback algorithm, implemented in software, controls the hyperthermia array phase shifters and focuses the transmitted radiation beam. In 10 to 15 iterations, the measured phantom data indicate rapid convergence of the adaptive focusing algorithm and significant increase of the focal region field strength due to the adaptive focusing. Two-dimensional E-field radiation pattern measurements were collected by scanning the E-field dipole probe antenna inside the muscle-equivalent liquid phantom. The measured, adaptively phase-focused radiation pattern data indicate a maximum useful heating depth of about 3 cm in a muscle-equivalent sugar/saline phantom having dielectric losses of 3 dB/cm.

14. SUBJECT TERMS		15. NUMBER OF PAGES
tumor heating	adaptive phased array	56
microwave hyperthermia	adaptive focusing	16. PRICE CODE
cancer therapy		

17. SECURITY CLASSIFICATION OF REPORT	18. SECURITY CLASSIFICATION OF THIS PAGE	19. SECURITY CLASSIFICATION OF ABSTRACT	20. LIMITATION OF ABSTRACT
Unclassified	Unclassified	Unclassified	Same As Report